FUNDAMENTALS OF THz TECHNOLOGY FOR 6G

White Paper | Version 01.02 | Dr. Taro Eichler, Robert Ziegler

dataTec

Mess- und Prüftechnik. Die Experten.

Ihr Ansprechpartner /
Your Partner:

dataTec AG
E-Mail: info@datatec.eu
>>> www.datatec.eu

ROHDE&SCHWARZ

Make ideas real

CONTENTS

1 INTRODUCTION

Terahertz (THz) waves have frequencies extending from 0.1 THz up to 10 THz or wavelengths between 3 mm and 30 μm. They fall in the spectral region between microwaves and optical waves. The prospect of offering large contiguous frequency bands to meet demand for extremely high data transfer rates in the Tbit/s range is making this region a key research area for next generation wireless communications (6G). Commercial deployment is expected around 2030.

Efforts to explore and "unlock" this frequency region require an interdisciplinary approach with close interaction with high frequency semiconductor technology for RF electronics but also encompassing alternative approaches using photonic technologies. The THz region also shows great promise for many application areas ranging from imaging to spectroscopy and sensing.

The objective of this white paper is to provide a concise overview of the fundamentals of THz waves and their properties for various applications with a focus on 6G communications.

Chapter 2 introduces key 6G performance requirements and research areas.

Chapter 3 discusses potential applications such as THz based communications and sensing. These applications will require extension of the frequency spectrum to frequencies above 100 GHz. There, interaction of the THz waves with matter has a strong impact on application scenarios.

Chapter 4 highlights various ways to generate THz radiation. Besides using electronic MMICs, alternative methods based on photonic technologies will play a key role in the future. Especially with the prospect of miniaturizing today's lab setups into photonic integrated circuits (PIC), these approaches could become mainstream.

With its established production processes and high level of integration, THz generation via electronics is currently still the dominant technology. Frequency limits are being further extended on a continuous basis. **Chapter 5** summarizes the current state of the art in high frequency semiconductor technologies.

At the 2023 ITU World Radio Conference (WRC23), additional frequency bands beyond 100 GHz are expected to be discussed and considered for allocation at the subsequent WRC27. Today's activities are now being pursued to demonstrate the full potential of THz communications in feasibility studies.

In order to fully exploit the THz potential for the development of future communications standards such as 6G, it is crucial to understand the propagation characteristics by performing channel measurements. Subsequent development of new channel models for these new communications frequency bands represents one of the first steps in the standardization process.

Chapter 6 describes channel propagation measurement concepts and presents some initial results from channel sounding campaigns at 158 GHz and 300 GHz at Rohde&Schwarz headquarters in Munich.

2 TOWARDS THE NEXT WIRELESS COMMUNICATIONS STANDARD 6G

2.1 From 5G to 6G – vision and key technologies

Setting up nationwide 5G networks with successive provision of new communications capabilities and services will keep the industry busy for many years. 5G has opened the door for new application scenarios such as Industry 4.0 with the representative service categories **enhanced mobile broadband (eMBB)**, **ultra-reliable low latency communications (URLLC)** and **massive machine type communications (mMTC)**. While 5G services will further continue to improve towards the 3GPP Release 18 evolution step, academia and industry have initiated research on the fundamentals of next generation wireless communications (6G). Commercial deployment is expected around 2030 and a pre-commercial launch could possibly occur one year earlier. Excellent overviews illustrating different perspectives on 6G visions and technologies are given, for example, in [1] [2] [3] [4] [5] [6] [7] [8] [9] [10]. Here, we highlight some of the key aspects.

The ITU Radiocommunication (ITU-R) Working Party 5D (WP 5D) began to develop a new draft recommendation document "IMT Vision for 2030 and beyond" in 2021 to define the framework and overall objectives for the future development of IMT2030+, which will eventually be called "6G". The first 3GPP standardization efforts are anticipated for 2023/24, starting with the definition of technical performance requirements. Definition of the standard is to be commenced from 2026/2027 onwards.

It is difficult to predict which applications and use cases envisioned by the industry will eventually be the main driver for the next generation wireless standard and which in turn will shape the system requirements (KPIs) and technologies for 6G. Among the potential application scenarios are, for example, holographic applications, extended realities XR (AR, VR, mixed realities MR) or digital twins, which pose extremely stringent requirements with respect to data transmission rate and latency. The vision is that in the 6G era, the digital, physical and human world will seamlessly fuse (cyber-physical fusion), leading to a connected society in which communications connects people, machines and virtual services with all of the necessary components of our daily life. The deployed sensors and actuators need to securely transfer and process data at extremely high rates to realize "immersive communications" of this kind.

Table 1 summarizes the estimated KPI requirements. For 6G, the targeted values are more stringent by a factor of approx. 10 times to 100 times compared to 5G and will pose new challenges for wireless communications and transport networks.

In certain time-sensitive control applications for synchronization (e.g. in industrial application environments such as factory automation), instead of the net latency it is important to have consistent and deterministic end-to-end latency with low fluctuations, i.e. low jitter. This is introduced as a new KPI [11] [12]. Space-time synchronization will allow time synchronization and mutual positioning by wireless technology for remote devices to work cooperatively [9].

Table 1: Expected enhancements of key performance indicators (KPI) from 5G to 6G

Jitter is a new KPI defining a limit for latency fluctuations for time-sensitive operations [11] [12].

Key performance indicators (KPI)	5G	6G	Improvement factor
Peak data rate (in Gbps)	10	100 to 1000	10 to 100
User experienced data rate (in Gbps)	0.1	1 to 10	10 to 100
User plane latency (in ms)	1	0.1	10
Connection density (in devices/km^2)	10^6	10^7 to 10^8	10 to 100
Reliability	99.999%	99.99999%	100%
Energy efficiency	$1\times$	$5\times$ to $100\times$	5 to 100
Spectral efficiency	$1\times$	$2\times$	2
Positioning (in cm)	20 to 100 in 2D	1 in 3D	20 to 100
Jitter, i.e. latency variations (in µs)	–	0.1 to 1000	–

The new 6G communications standard should also be an important foundation for a human-centered, sustainable and inclusive society [9]. Living space will be expanded and communications will also need to cover those areas. For example, the United Nations Sustainable Development Goals (SDG) offer a guideline in the form of a footprint for energy and resources as well as equal, affordable and scalable provision of services to remote areas. The current network energy footprint is already a concern – not solely due to the environmental impact but also because of its major impact on network operator OPEX. In order to cope with the exponential increase in data communications, the energy per transferred bit must be reduced.

2.2 6G research areas

Figure 1 provides an overview (albeit not comprehensive) of the main 6G research areas that have been identified to realize the vision and enable use cases for future wireless communications.

While some of the technologies represent evolutionary changes already used in previous generations, other technologies are disruptive and could unlock potential beyond Shannon's limits.

Figure 1: 6G research areas

Ultra-high-speed channel coding

New waveforms, multiple access

Ultra-massive MIMO

Full-duplex communications

New network topologies

THz sensing and communications

Photonic technologies/VLC

Reconfigurable intelligent surfaces

Distributed computing

AI and machine learning
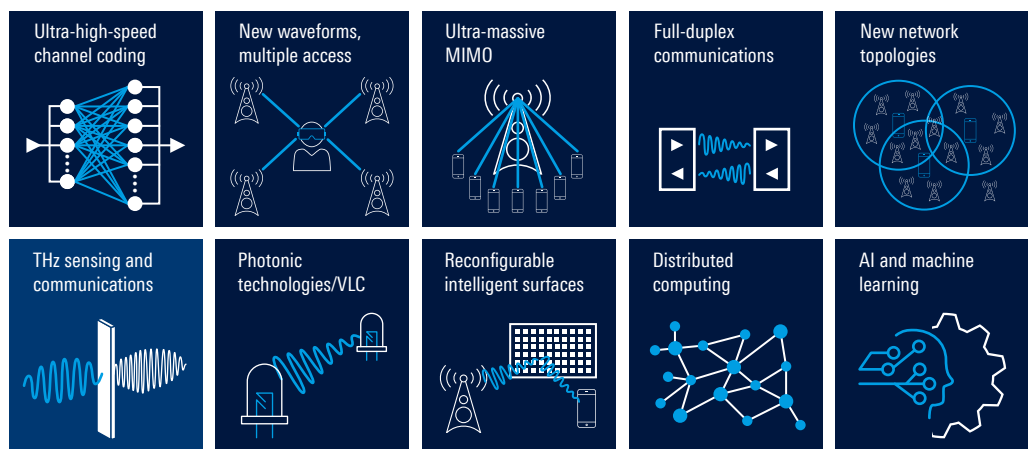
Evolution of technologies already used in previous generations

Some evolutionary technology steps, such as new waveforms as alternatives to OFDM or full-duplex operation, were previously discussed for 5G but were not included in the standard.

Ultra-high-speed channel coding

Channel coding is a fundamental component in wireless communications for correcting transmission errors and is thus a key to reliability. At the same time, it is a complex part of baseband processing, and the new KPIs in terms of very high throughput, reliability, low power consumption, etc. require enhancements of modern channel coding schemes such as Turbo, LDPC and polar codes.

New waveforms and multiple access

Efficient operation of wireless systems is highly dependent on adequate waveform design. While OFDM remains a strong candidate for 6G waveforms, alternative application-specific waveforms or unified scalable waveforms need to be explored, for example, for joint communications and radar sensing. Moreover, the different spectrum ranges, device characteristics (phase noise, PA power efficiency) and system characteristics (signal bandwidth) must be taken into account. A number of new waveforms are under consideration, including orthogonal time frequency space modulation (OTFS) for high mobility scenarios with large Doppler spreads. Furthermore, single carrier waveforms may play a more dominant role to fulfill the requirements for power efficiency in future devices. To allow more flexible use of wireless channels, it could be beneficial to relax the orthogonality constraint, as is realized for non-orthogonal multiple access (NOMA).

Ultra-massive MIMO

Massive MIMO was introduced in 5G. The trend towards even higher frequencies and shorter wavelengths makes it possible to increase the number of antennas in a small area to provide more directed beams. This is also needed to compensate for higher losses at high frequencies.

Another means to increase spectral efficiency is to apply self-interference cancellation techniques enabling **full-duplex communications** for in-band bidirectional communications and relaying.

New network topologies

The cellular layout used in the current network architecture is designed to minimize interference at the cell borders between cells. In order to achieve ultra-high-speed, high capacity (with needed improvement **in particular on the uplink to connect to the "cloud AI brain"**) and high reliability communications, however, it is ideal to communicate at short distances via a low-loss path and increase the redundancy over multiple communications paths. One possibility for such a spatially distributed topology involves **cell-free networks** where base stations – distributed over a large area – coordinate coherent joint transmission to provide service to each user. This approach will lead to a higher signal-to-noise ratio and gain and a more consistent quality of experience for users at different locations. However, the implementation entails high computing complexity and tight synchronization requirements between the base station locations along with the exchange of large amounts of data between the sites.

In order to provide new services to drones, aircraft, ships and space stations/satellites and thus bring coverage to remote areas, sea and space, it is necessary to extend the network coverage three-dimensionally. Thus, the vertical direction is also included in addition to horizontal deployment. Such ubiquitous communications could be realized, for example, with non-terrestrial networks (NTN) that utilize drones (high altitude platform stations or HAPS in the stratosphere at 20 km altitude) and low earth orbit (LEO) satellite constellations as mobile base stations in the sky.

THz communications and sensing

One of the key technology concepts for 6G – albeit just one of the 6G enablers – is the use of **THz waves for communications and sensing. These THz applications and technologies will be discussed in detail in the following chapters**. Unlocking the potential of the sub-THz and THz frequency regions (100 GHz to 3 THz) with the available extremely high bandwidths of several GHz represents a technological way forward. Besides ultra-high data rates in wireless communications, this would also benefit sensing and imaging applications as well as possible future medical diagnostic procedures.

The concept of **joint communications and sensing (JCS)** – sometimes called integrated communications and sensing (ICAS) – comprises a system definition to natively support both applications as part of the physical layer design, i.e. the jointly used waveforms and the network architecture. It is not limited to THz frequencies but also encompasses the millimeterwave (mmWave) range. The wide bandwidths will also benefit high-precision sensing applications. These could include not only positioning, object detection or high-resolution radar but also spectroscopy-type analysis – of particular interest for environmental sensing.

Photonic technologies and visible light communications (VLC)

Optical wireless communications (OWC) is already used in some areas as a complementary technology to satisfy the requirements for additional capacity. It has the potential to become more prevalent as it combines high speed and high fidelity with low deployment costs. Key advantages over radio frequency based access networks is the availability of approximately 300 THz of license-free bandwidth carried on visible and IR wavelengths, robustness against interference and secure communications, e.g. in indoor environments where the radiation does not penetrate walls. Free-space optical communications (FSO) with infrared wavelengths uses modulated laser diodes for transmitting information through free space, e.g. as a backhaul solution or for space based communications between satellites. However, it is affected by weather conditions, atmospheric turbulence and especially fog.

In **visible light communications (VLC)**, also known as "light fidelity" (LiFi), data is transmitted via high bandwidth intensity modulation of commercial LEDs used for lighting. A photodiode serves as the receiver. This is a cost-efficient approach that allows easy integration into existing infrastructure primarily for line of sight indoor applications [13].

The stringent 6G KPIs will also drive the **evolution of the future transportation network in wireless networks**. For example, the Innovative Optical and Wireless Networks Global Forum (IOWN GF) aims to develop technologies for a computing and communications network architecture to achieve scalability, elasticity (regarding sporadic workload fluctuations), energy efficiency and latency manageability at the same time [11]. **Photonic technologies** can help to cope with these challenges: The proposed open all-photonic network (APN) could help to streamline data transfer and processing and realize a large capacity, low latency and low energy consumption infrastructure. For example, it enables a direct end-to-end optical path connection across domains/hierarchies between any user terminals or points in the network with minimal photoelectric conversion to provide low latency service. Integrated optical devices (photonic integrated circuits, PIC) could provide the routing and termination functions to implement such an end-to-end all-optical connection. Furthermore, extrapolating the trend for the capacity demand increase in the 2030s Pbit/s class communications capacity will be required for long-haul transmission. The limit of current single-mode fibers (SMF) is around 100 Tbit/s. The limit can be further increased with ultra-wideband optical transmission using multi-core fiber transmission technology where multiple cores are embedded into a single glass fiber and by further increasing the number of wavelengths through multiplexing and adding new optical bands.

Another photonic technology that was first demonstrated conceptually more than 25 years ago but has recently attracted increasing interest is **quantum communications** (and quantum networks). This could play a complementary role for 6G as one possibility to ensure **trustworthiness for ultra-secure and reliable communications**. Quantum communications provides an inherently secure means of **quantum key distribution (QKD)** through the exchange of entangled photons. These digital keys would subsequently be used for conventional encrypted transmission. Such technologies could be integrated and transmitted via optical fiber. However, free-space QKD between a satellite and earth has also been demonstrated [14], which could serve as the basis for realizing a future quantum communications network [15].

Reconfigurable intelligent surfaces (RIS) and metamaterials

The use of RIS when installed on building facades or in indoor environments could direct the energy of a wireless signal towards a certain point, thus providing better coverage in non line of sight environments and reducing energy consumption.

Since the early days of wireless communications, the propagation channel has been considered as a randomly and – depending on the scenario – dynamically changing entity between the transmitter and receiver. It has the effect of degrading the quality of the received signal in an uncontrollable fashion owing to the surrounding environment and objects as well as the mobility of the receiver. One of the basic assumptions in communications theory (from which, for example, the Shannon theorem is derived) is that the propagation channel is a given within the communications system and cannot be influenced. The use of reconfigurable intelligent surfaces (RIS) could provide a tool to change the propagation channel and thus introduce a new programmable entity into the wireless communications network with the prospect of extending the boundaries beyond the Shannon limit.

A **reconfigurable intelligent surface** (also referred to as an **intelligent reflecting surface, IRS**) is a planar structure that is designed to have properties that enable dynamic control of electromagnetic waves. An IRS consists of a large number of low-cost, passive (and thus low energy) elements, each reflecting the incident signal with a certain phase shift to collaboratively achieve beamforming and suppress interference at one or more designated receivers. The building blocks of such an RIS are so-called metamaterials that are – in contrast to a material with properties based on its atomic constituents – engineered structures designed to interact with electromagnetic radiation in a desired fashion and with special properties. They usually comprise an array of structures smaller than the wavelength of interest.

Targeted RIS scenarios are ultra-dense network deployments predominantly in indoor environments (malls, airports, stadiums or industrial/factory environments).

In October 2021, the European Telecommunications Standards Institute (ETSI) launched a new industry specification group (ISG) on reconfigurable intelligent surfaces (ISG RIS) for reviewing and establishing global standardization for RIS technology [16]. Smart repeaters, as they are currently discussed in 3GPP for Release 18, may be the stepping stone towards reflective intelligent surfaces.

Distributed computing and artificial intelligence (AI) communications systems

Although future 6G application scenarios still have to be defined, it is evident that performance requirements will be even more demanding compared with 5G in terms of data rate, latency, spectral efficiency, security, reliability and energy consumption. This will also impact the **processing architecture: information technologies and communications technologies will further merge**, i.e. the processing of large amounts of data will take place in distributed systems in the network and not necessarily in the end user device. This leads to challenging data rate and latency requirements. Computing power could be offloaded to the cloud or edge networks separate from devices (thus allowing cheaper terminals).

In the traditional "von Neumann" computing architecture, the computing unit (CPU) and the memory are separated. Moving large amounts of data between the CPU and memory becomes a bottleneck in terms of energy consumption and latency. New approaches in computing architecture such as neuromorphic computing take inspiration from the human brain for energy-efficient processing with low latencies. There, the computational tasks are performed in the memory itself. The human brain, for example, has very good computing power versus power consumption (a total of 20 W to 30 W).

AI-related tasks rely heavily on computational processing power. Further upscaling of the performance of graphical processing units (GPU) will eventually be limited by the available energy. For such tasks, analog AI cores for in-memory computing are particularly suitable. New concepts such as an analog 3D cross-point array of resistors, used as non-volatile memory to store the weights (e.g. for convolutional neural networks), can be used to calculate matrix-vector calculations (the prevalent type of calculation for neural networks) in parallel [17] [18].

AI and machine learning

Already today, artificial intelligence (AI) and machine learning (ML) are being used for self-management and control operations for a number of network applications. These include the initial network planning phase, network control and optimization such as traffic management, dynamic spectrum management as well as predictive and adaptive resource allocation.

It is expected that in the future, AI will become an integral part of all areas of the wireless communications system. This could include a physical layer design that adapts to the specific propagation channel and environmental conditions with the possibility of end-to-end optimization – instead of optimization of each component of the radio transmission chain [19]. To cope with the increase in complexity of future 6G networks regarding device types, spectrum ranges and flexible network topologies such as cooperative mesh type networks, AI and machine learning will play an important role for 6G deployment and operation. This will make it possible to optimize system performance in terms of maximizing user experience and cost efficiency and minimizing energy consumption.

Recently, ETSI has also begun to focus on AI in terms of AI based testing and testing AI based systems from the regulatory perspective [20]. Relevant working groups are the ETSI Technical Committee (TC) Core Network and Interoperability Testing (INT) and the ETSI Technical Committee (TC) Methods for Testing and Specification (MTS).

3 PROPERTIES AND APPLICATIONS OF THz WAVES

3.1 New 6G spectrum at mmWave and THz frequencies

On the way to the terahertz spectrum

Whereas 5G pioneered the use of millimeterwave frequencies with large bandwidths up to 400 MHz per component carrier to enable the transmission rates necessary for demanding real-time applications such as wireless factory automation, the nascent 6G technology is aiming at significantly higher transmission rates and lower latencies.

However, large contiguous frequency ranges for ultra-high data rates with bandwidths of several GHz are only available in the subterahertz and terahertz range, i.e. above 100 GHz (Figure 2).

The Shannon-Hartley theorem, which gives a boundary for the maximum achievable channel capacity (under the influence of noise) $C = B \cdot \log_2(1 + S/N)$, where C is the capacity in bit/s, B the bandwidth in Hz, and S/N the signal-to-noise ratio, states that the maximum achievable data rate scales proportional to the bandwidth B [21]. This was the motivation for 5G to extend the frequency region into the mmWave range as frequencies below 6 GHz are already heavily in use. In order to increase data rates even further for future wireless standards such as 6G, even higher frequency bands up into the THz spectrum – where large contiguous bandwidths of several GHz are available – are under consideration. Figure 2 shows the different frequency ranges allocated or considered for future wireless communications.

Figure 2: New spectrum for 5G and 6G

A huge spectrum will be available in the mmWave and THz frequency range. Spectrum of frequency bands available for wireless communications. The 5G bands in FR1 and FR2 are distributed over the range below 71 GHz. 6G research is concentrating on the D and H bands.
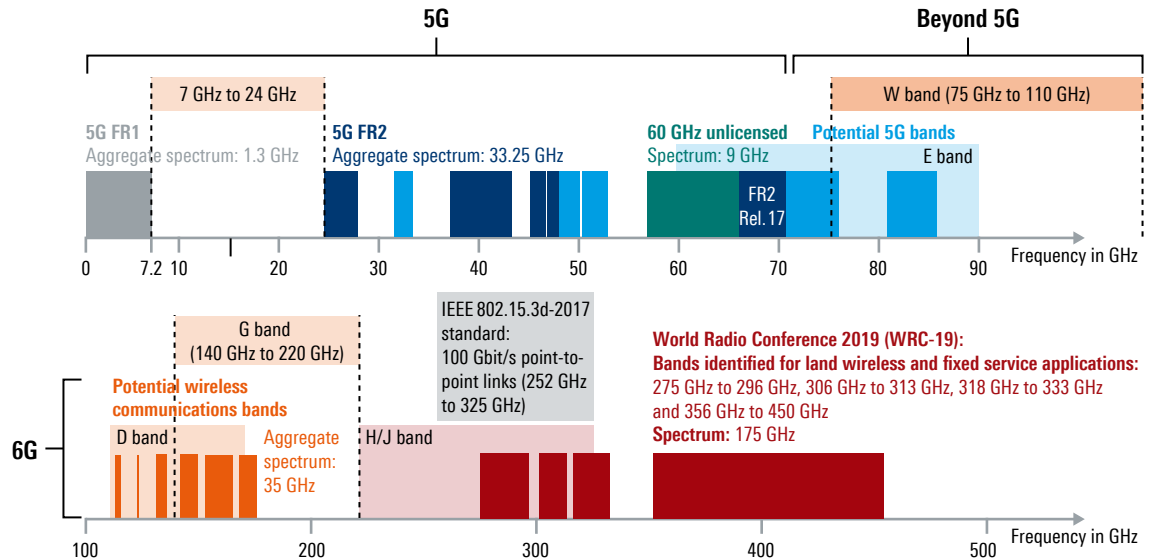
Up to 4G (LTE), only the frequency region below 6 GHz was used for wireless communications. This frequency range still plays a key role because of its favorable propagation conditions and the large cell sizes that can be achieved as a result.

In the 3GPP 5G NR nomenclature, this frequency region is called 5G FR1 (410 MHz to 7.125 GHz). This region also includes LTE and Wi-Fi such as Wi-Fi 6 (IEEE 802.11ax) and Wi-Fi 7 (IEEE 802.11be).

In 3GPP Release 17, 5G FR2 (in dark blue) has been assigned up to 71 GHz (24.25 GHz to 71 GHz).

For the evolution of 5G ("Beyond 5G" in Figure 2), even higher frequencies above 71 GHz up to 100 GHz are under consideration: The light blue colored bands are frequency regions considered for future wireless communications by the International Telecommunication Union (ITU) World Radio Conference 2019 (e.g. 81 GHz to 86 GHz). Although considered initially, the 80 GHz frequency region was not approved for IMT-Advanced (5G). This frequency region also contains the 60 GHz unlicensed band (the E band extends from 60 GHz to 90 GHz).

Sub-THz bands

In order to enable terabit-class data rates for 6G, even higher bandwidths are necessary. However, they are only available in the range beyond 100 GHz. Potential new frequency bands have been identified in the D band (110 GHz to 170 GHz), G band (140 GHz to 220 GHz) and in the H/J band (220 GHz to 330 GHz).

The ITU [22] radio regulations document summarizes the conclusions of the radio regulations adopted by the World Radiocommunication Conference of 1995 (WRC-95) and reviewed by subsequent World Radiocommunication Conferences (WRC-97, WRC-2000, WRC-03, WRC-07, WRC-12, WRC-15 and WRC-19). As stated on pp.185 in [22], the region 275 GHz to 3 THz is not officially allocated. However, the footnote 5.564A comments on the operation of fixed and land wireless service applications in frequency bands in the range 275 GHz to 450 GHz, which were added at ITU World Radio Conference 2019 (WRC19). From the final acts of the WRC19 [23]: "For the operation of fixed and land wireless service applications in frequency bands in the range 275 GHz-450 GHz: The frequency bands 275-296 GHz, 306-313 GHz, 318-333 GHz and 356-450 GHz are identified for use by administrations for the implementation of land wireless and fixed service applications, where no specific conditions are necessary to protect Earth exploration-satellite service (passive) applications."

Standardization activities are currently also underway at the IEEE where an interest group is introducing a standard for 100 Gbps at these frequencies [24]. This standard specifically targets the frequency range from 252 GHz to 325 GHz with signal bandwidths up to 69.12 GHz.

Development of terahertz-range bands for wireless backhaul/access is already happening in the W band spectrum (75 GHz to 110 GHz) around 95 GHz. The next extremely high candidate band, the D band at 110 GHz to 170 GHz, is being eyed by base station infrastructure vendors. 6G research efforts are now concentrating on the D band and the H/J band around 300 GHz. Since the agenda for WRC27 will be fixed at WRC23, activities are now in full swing to demonstrate the full potential of THz communications through feasibility studies and channel propagation measurements (Chapter 6) before WRC23 in 2023.

Beyond 7 GHz (7 GHz to 24 GHz)

Despite strong interest in the sub-THz band, the frequency range 7 GHz to 24 GHz that lies in the gap between FR1 and FR2 still offers potentially large blocks of available spectrum (Figure 2). It could provide a "sweet spot", offering the possibility for higher order MIMO in a smaller package (compared to FR1) but more favorable propagation characteristics in comparison to the bands operating in FR2. Therefore, this region could be a complementary 6G candidate.

3.2   THz applications

3.2.1   A plethora of applications yet to be explored

Terahertz (THz) waves lie in the portion of the frequency spectrum between the realms of optics and microwaves. One of the early drivers of THz spectroscopy was the need for high-sensitivity instrumentation for astrophysical observations and environmental monitoring. However, recent technological innovation in photonics and nanotechnology is now enabling THz research to be applied in many more sectors.

Spectroscopy and imaging: THz waves show great promise and are already used for many applications in spectroscopy and high-resolution imaging since many forms of condensed matter, molecular compounds, vapors and gases possess different physical features resonant with THz waves [25] [26]. Many substances and complex molecules can be easily identified using THz spectroscopy techniques such as pharmaceuticals, biomolecules and proteins. Figure 3 shows an example of a common drug molecule where the characteristic absorption lines at THz frequencies can be used to distinguish between the two main molecule variants. Security could also benefit from such a sensor as many common explosives or narcotics could be identified by their spectral "fingerprint" [26]. Terahertz waves allow nondestructive product inspection and can "look inside" plastics, textiles, paper, etc. Unlike X-rays, terahertz waves do not have any ionizing effect and are generally considered biologically innocuous. Thus, they do not require any additional safety measures when used, for example, for security scanning.

Communications: Data traffic is increasing exponentially and internet protocol traffic surpassed 100 exabytes (1 Ebyte = 10^{18} byte) per month already in 2017. This is expected to have tripled in 2022. Since the fastest-growing part of data traffic is related to wireless channels, such an increase in network capacity requires much higher wireless transmission data rate links. The prospect of offering large contiguous frequency bands to meet the demand for extremely high data transfer rates in the Tbit/s range with low latency makes it a key research area for 6G wireless communications – also in the context of joint communications and radar sensing.

Sensing and positioning: There is also a concept emerging that uses wireless frequencies for both communications and sensing capabilities, namely joint communications and sensing (JCS, Chapter 2.2). Terahertz frequencies would not simply carry communications data, but could work much like a highly precise radar system to detect objects. In this way, THz sensing can provide high-resolution maps of the environment and positioning information at centimeter and sub-centimeter level accuracy. This could be applied, for example, in factories for industrial control and monitoring applications such as robotics or virtual reality.

Figure 3: Application of THz waves in communications and sensing, spectroscopy and imaging

The left picture shows a D band radar chip from the Leibnitz Institute for High Performance Microelectronics (IHP). Center: Analysis of the terahertz spectra from a sample of diclofenac acid can distinguish between the two chief forms, or polymorphs, of the drug. Right: Microwave imaging picture captured with the R&S®QPS100 (70 GHz to 80 GHz).

Communications and sensing	Spectroscopy	Imaging
▶ Ultra-high-speed communications ▶ Fusion of communications and sensing (radar) capabilities	▶ Material analysis ▶ Analysis of the terahertz spectra from diclofenac acid can distinguish between the two chief forms of the drug	▶ Nondestructive imaging (with R&S®QPS100 security scanner) ▶ Production line (final assembly test)

3.2.2 THz waves for atmospheric remote sensing and astrophysics applications

According to the Planck radiation law, the energy of a terahertz photon corresponds to a temperature of a few Kelvin up to few tens of Kelvin. THz astronomy research therefore explores the cold universe such as molecular clouds of interstellar matter. Of special interest are regions where new stars are born. In 1970, carbon monoxide (CO) was detected as the first molecule in an interstellar cloud with a transition in the terahertz range at 115 GHz [27], commencing the age of THz astronomy.

Radiometer Physics GmbH (RPG, a Rohde & Schwarz company) originated from the Max Planck Institute for Radio Astronomy and the NASA Jet Propulsion Laboratory and has been involved in this scientific research from early on. The company has a long history of providing cutting-edge instruments for THz space R&D projects for remote sensing, millimeterwave, sub-mm and THz instruments and components up to 2 THz.

The absorption and emission properties of molecular species (see Figure 7 for an example for the earth's atmosphere) are of particular interest for scientists and meteorologists who are investigating the dynamics of the atmosphere of planets (Earth, Jupiter, Venus, Mars, etc.) using millimeterwave and submillimeterwave instruments. Depending on the applications and science objectives, various types of **passive instruments** operating typically in the 18 GHz to 664 GHz range for **radiometers** and 0.3 THz to 1.2 THz range for **spectrometers** are used, as well as **active instruments** operating in the 35 GHz to 94 GHz range for **FMCW radars** and at 166 GHz for **scintillation radiometers**. These instruments can be operated from ground based stations or from space onboard satellites. Figure 4 shows examples of a passive radiometer, active sources and radar instruments for atmospheric remote sensing, planetary science and astrophysics purposes.

Over the past ten years, RPG has developed THz heterodyne receivers in the 183 GHz to 664 GHz range for the Ice Cloud Imager (ICI) [28], a conical scanning multi-channel radiometer developed by Airbus-ASE for the European Space Agency ESA/EUMETSAT Meteorological Operational Satellite Second Generation program (MetOp-SG, Figure 4, left). It is a European undertaking providing weather data services (including, for example, ocean surface wind vectors and land surface soil moisture) to monitor the climate and improve weather forecasts for the 2023 to 2043 timeframe. Water vapor, carrying energy as latent heat, is playing a pivotal role in fueling destructive storms and accelerating climate change. With the increase in the oceanic and atmospheric temperature, the amount of vapor in the atmosphere globally has increased by about 4 % since the

mid-1990s [29]. Since this trend acts as an amplifier for global warming and gives rise to more rapidly intensifying storms, close monitoring of temperature, vapor and winds is extremely valuable for predicting weather patterns.

For the ESA Jupiter Icy Moon Explorer (JUICE) program (Figure 4, center), RPG developed high-power sources in the 132 GHz to 158 GHz range for the submillimeterwave instrument (SWI) [30], a dual-channel 0.6 THz to 1.2 THz spectrometer developed by the Max Planck Institute for Solar System Research (MPS). The JUICE mission is planned for launch in 2023. It will spend at least three years making detailed observations of the giant gaseous planet Jupiter as well as three of its largest and water-rich moons (Ganymede, Callisto and Europa). Also of interest is the characterization of Jupiter's atmosphere and magnetosphere.

The technology underlying both instruments (for the MetOp-SG and JUICE mission) relies heavily on GaAs semiconductor devices (amplifiers, multipliers, mixers) and high-precision manufacturing and assembly techniques (horn antennas, RF modules) that were qualified in accordance with the most stringent requirements required for space missions.

Figure 4: Examples of THz wave applications in the field of atmospheric remote sensing and astrophysics
Left: Space based passive radiometer ice cloud imager (ICI) multi-channel receivers (RX) operating in the 183 GHz to 664 GHz range (delivered flight model) [28] (photo courtesy of RPG/Airbus/ESA/EUMETSAT). Center: Example of 132 GHz to 158 GHz LO sources (TX) developed for the submillimeterwave instrument (SWI) spectrometer for planetary science onboard the ESA JUICE mission [30]. Right: 94 GHz FMCW radar instrument for cloud sensing and 166 GHz scintillation radiometer instrument for field evaporation sensing.

► ESA MetOp-SG program
► Ice cloud imager instrument
► Multipixel, 183 GHz to 664 GHz
  FE heterodyne receivers

► ESA JUICE program
► THz spectrometer instrument
► 150 GHz high-power LO sources and THz antennas

3D cloud and precipitation radar
(image: EPFL)

Passive (radiometer)
► Humidity and temperature profiler
► Water vapor and/or ice cloud remote sensing
► Single and dual polarization radiometers
► Ground based or space based instruments

Passive (spectroscopy sources)
► Atmospheric spectroscopy
  (e.g. water vapor, methane)
► Astrophysics and radio astronomy
► Multi-channel instruments
► Single pixel and/or interferometry

Active (radar)
► Frequency modulated continuous wave
  cloud radar
► Scintillation radiometer (TX/RX system)

3.3 THz waves for communications: What are possible use cases?

Use absorption windows, power and antenna arrays for directivity

The technical challenges of millimeterwaves are even more pronounced in the terahertz range. This includes higher path loss and shorter range. However, similar to millimeterwaves in 5G, these problems can be mitigated by focusing the waves through beamforming. The shorter wavelengths also have the advantage that a larger number of antennas can be fitted into a small package in order to produce highly pinpointed beams.

One of the main use cases for ultra-high-speed communications at THz frequencies involves high-capacity front- and backhaul point-to-point (quasi-static) communications links also for infrastructure in remote locations (using high gain antennas or antenna arrays) or "last-mile" connections. The expectation is that capacities up to 100 Gbps can be supported over a distance of a few kilometers [31]. Furthermore, the narrow beams could also enable very dense deployment of communications devices. Another applications include short-range communications such as ultra-fast kiosk downloads (e.g. at vending machines) or chip-to-chip communications (Figure 5).

Today, data centers are an integral part of enterprise computing infrastructures. Contemporary data center networks mostly rely on copper or optical fiber cables for intra-rack or inter-rack network connections. This is associated with high cabling complexity. THz wireless links could greatly increase design flexibility and reduce costs [32].

While both outdoor and indoor terahertz use cases are feasible, indoor use cases are likely to dominate terahertz applications. In indoor settings, the short range and weak penetration capabilities of the terahertz spectrum are an advantage. For example, terahertz communications can be highly secure since it can be limited to a specific indoor space.

Figure 5: THz communications use cases

Backhaul/fronthaul links	Kiosk and intra-device communications	Wireless link in data centers
► Ultra-high-speed communications ► Backhaul/fronthaul P2P connections ► Infrastructure in remote locations	► Ultrafast download of prefixed content (e.g. UHD video, music) at specific locations (vending machines, train stations) ► Chip-to-chip communications	► Communications inside data centers: remote memory can increase design flexibility and reduce cost by extending CPU memory distance

3.4   The electromagnetic spectrum and its applications

Figure 6 shows the electromagnetic spectrum and various applications ranging from broadcast and cellular communications at the lower frequency end to X-ray imaging and gamma ray therapy at the highest energies (and thus frequencies). The terahertz spectrum lies on the borderline between electronics and photonics. The definition of the THz band varies in literature, but the IEEE and ITU definitions are 300 GHz to 3 THz (THF or tremendously high frequency), just above the millimeterwave frequency range (30 GHz to 300 GHz; EHF or extremely high frequency) and the microwave range (3 GHz to 30 GHz; SHF or super high frequency). However, in publications the range above 100 GHz up to 10 THz is often denoted as THz frequencies. The frequency range from 100 GHz to 300 GHz is also often called the sub-THz region.

Figure 6: The electromagnetic spectrum and applications with the terahertz spectrum on the borderline between electronics and photonics
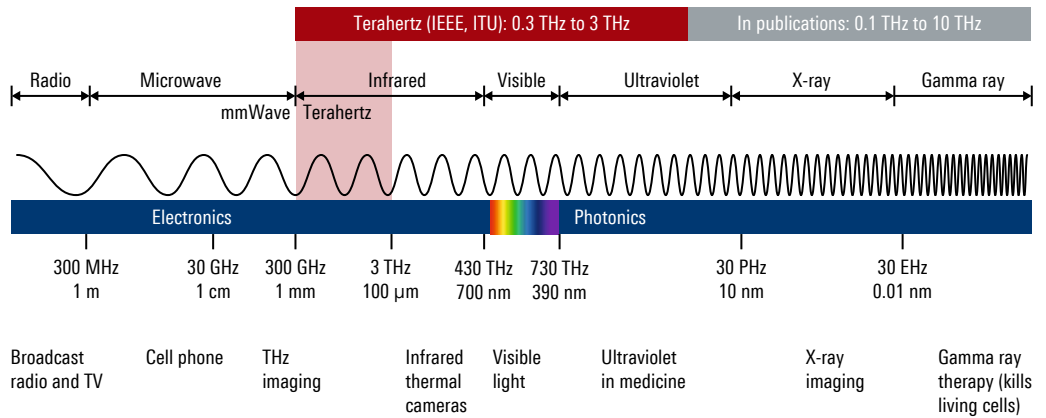
3.5   Interaction of terahertz waves with matter

The energy of terahertz waves is comparably low (by a factor of $100\times$ to $1000\times$ smaller than optical frequencies) and does not initiate any chemical structure changes. It lies in the region of molecular rotational transitions of gas molecules and vibrational transitions of weak bonds. Terahertz waves can thus propagate through dry, nonmetallic and nonpolar materials with low attenuation. This ability, combined with its small wavelength (versus microwaves) and photon energy (versus X-rays), also makes THz waves an ideal option for nonionizing medical imaging, such as burn injury assessment or skin cancer diagnosis.

Figure 7 shows the specific atmospheric attenuation within the mmWave and THz spectrum. The resonance frequencies reflect the rotational excitation spectra of various molecules present in the atmosphere. The atmospheric attenuation increases steadily with increasing operating frequency. Between these resonance frequencies, there exist a number of "atmospheric windows" which can be used for various applications. Furthermore, the characteristic water vapor and ice absorption line at 183 GHz (in the G band; 140 GHz to 220 GHz) is exploited in earth and planetary exploration for remote humidity sensing (detection of ice). An example of radio-astronomical observations in the sub-THz band is the first ever direct picture of a black hole in the center of the galaxy M87. It was observed at 230 GHz by the Event Horizon Telescope (EHT) array by coherently combining the detected signals of radio telescopes distributed over different locations around the earth [33].

Figure 7: Specific atmospheric attenuation within the millimeterwave and THz spectrum

At air pressure of 1013 hPa, temperature of +15 °C and water vapor density of 7.5 g/m³. The rotational excitations of different molecules present in the atmosphere (i.e. water, oxygen) are reflected in the absorption spectra.
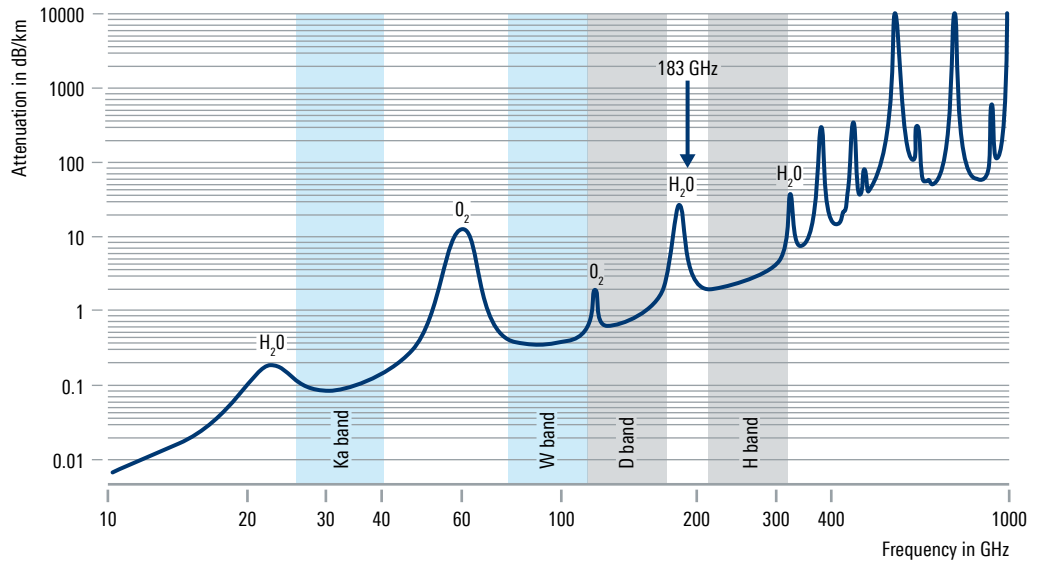
mmWaves and THz waves for wireless communications links

As shown in Figure 2, the frequency bands at 24 GHz to 30 GHz and 37 GHz to 40 GHz establish the mmWave region for 5G cellular networks. Furthermore, frequencies from 43 GHz to 50 GHz and around 60 GHz are used for satellite communications links. The increased propagation loss at 60 GHz owing to the resonance of oxygen molecules offers the possibility of establishing intrinsically secure wireless links with high data throughput for indoor applications (WLAN systems).

THz challenges: path loss for frequencies above 100 GHz

The next generation communications standard 6G is expected to also rely heavily on components that operate in the frequency range beyond 100 GHz such as the D band (110 GHz to 170 GHz) or the H/J band (220 GHz to 330 GHz).

Free-space path loss is proportional to the square of the signal frequency ν. A link at 280 GHz, for example, has 20 dB additional path loss compared to a link at 28 GHz.

However, there is a common misconception that increasing the carrier frequency of a wireless link will inevitably lead to a significantly higher channel loss. This is true only under the assumption that both the transmitter (TX) and receiver (RX) antennas are omnidirectional. The path loss in the THz band can be overcome by using very large antenna arrays at the base station, i.e. ultra-massive MIMO (Figure 1).

The **free-space path loss (FSPL)** of a wireless link is described by the **Friis equation**

$$FSPL = \frac{P_{TX}}{P_{RX}} = \frac{1}{G_{RX} \cdot G_{TX}} \left(\frac{4\pi d}{\lambda}\right)^2 \propto \nu^2$$

where d is the distance between the TX and RX antenna, λ is the operating wavelength, and G_{RX} and G_{TX} are the antenna gains of the transmitter and receiver, respectively. Given that the distance between TX and RX as well as their antenna gains are fixed, the FSPL value increases quadratically with increasing frequency $\nu = c/\lambda$. Figure 8 (left) illustrates this relationship, i.e. the FSPL versus the distance between TX and RX at three different frequencies for the case in which the antennas are omnidirectional ($G_{RX} = G_{TX} = 1$).

Figure 8: Theoretical Friis free-space path loss for mmWave wireless links

Left: Scenario where both TX and RX are omnidirectional. Right: Scenario where both TX and RX have directional antennas with a fixed effective aperture size of 1 cm².
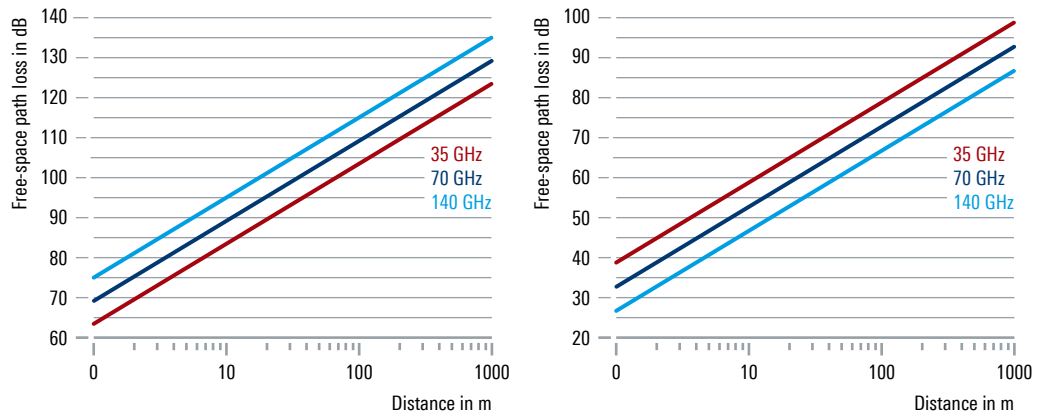
The antenna gain G_{ant} depends on the effective aperture A_{eff} of the antenna, which is proportional to its physical size, as well as on the wavelength:

$$G_{ant} = \frac{4\pi A_{eff}}{\lambda^2}$$

A directional antenna with a fixed effective aperture of 1 cm² has theoretically an antenna gain of 12.3 dBi, 18.4 dBi and 24.4 dBi when operated at frequencies of 35 GHz, 70 GHz and 140 GHz, respectively. With constant physical dimensions of the antennas, the antenna gain increases quadratically with increasing frequency.

Combining the last two equations, we can conclude that by using a directional antenna with a fixed effective aperture at either the transceiver or receiver, the FSPL is independent of the carrier frequency.

Therefore, employing highly directional and steerable antennas should enable wireless communications links operating at higher frequencies (with higher bandwidth and throughput) without a significantly reduced signal-to-noise ratio due to atmosphere-induced attenuation when compared with systems at lower carrier frequencies.

4 THz GENERATION AND ANALYSIS BY ELECTRONIC AND PHOTONIC TECHNOLOGIES

4.1 From electronics to photonics

During the past two decades, terahertz (THz) science – occupying the frequency gap between the worlds of microwave electronics and photonics – has attracted increasing interest due to the exciting opportunities that exist in the fields of sensing, imaging and data communications. Since the pioneering work nearly 100 years ago to create a link between the electrical and optical/infrared regions, development of efficient, stable and compact THz sources and receivers has been actively pursued and has made THz science a practical reality.

4.2 Closing the "THz gap"

In communications, the frequency range 0.1 THz to 10 THz is still a rather untapped region. However, research in this area has recently attracted increasing interest because these high carrier frequencies are associated with the promise of unprecedented channel capacities.

For a long time, it was difficult to generate intensive, directional terahertz radiation and the terahertz range was considered the final frontier in the electromagnetic spectrum. This main technical constraint, the so-called "THz gap", is shown in Figure 9 where THz emission power is plotted as a function of frequency for various electronic and photonic devices. Certain of these examples will be discussed in greater detail later. Clearly, there is a power drop visible towards the THz frequency spectrum in the region of 0.1 THz to 10 THz.

THz frequencies are too high for electronic devices, mainly due to excessive loss and limited carrier velocity. On the other hand, they are too low for photonic devices due to the lack of materials with a sufficiently small bandgap (see Chapter 4.4).

Despite the significant efforts that have been made in electronics (e.g. high-mobility semiconductor materials) and optics (e.g. a quantum-cascade laser with cryogenic cooling), the available power around the THz region is still much lower than in other spectral regions. A similar trend also occurs in signal detection where such a gap keeps this two-decade spectrum isolated from our spectrum-congested world.

Figure 9: THz emission power as a function of frequency [34]

Solid lines are for conventional THz sources; IMPATT diode stands for impact ionization avalanche transit-time diode, MMIC stands for microwave monolithic integrated circuit, TUNNET stands for tunnel injection transit time. Ovals denote recently developed THz sources. THz-QCL: quantum cascade laser, RTD: resonant tunneling diode, UTC-PD: uni-traveling carrier photo diode.
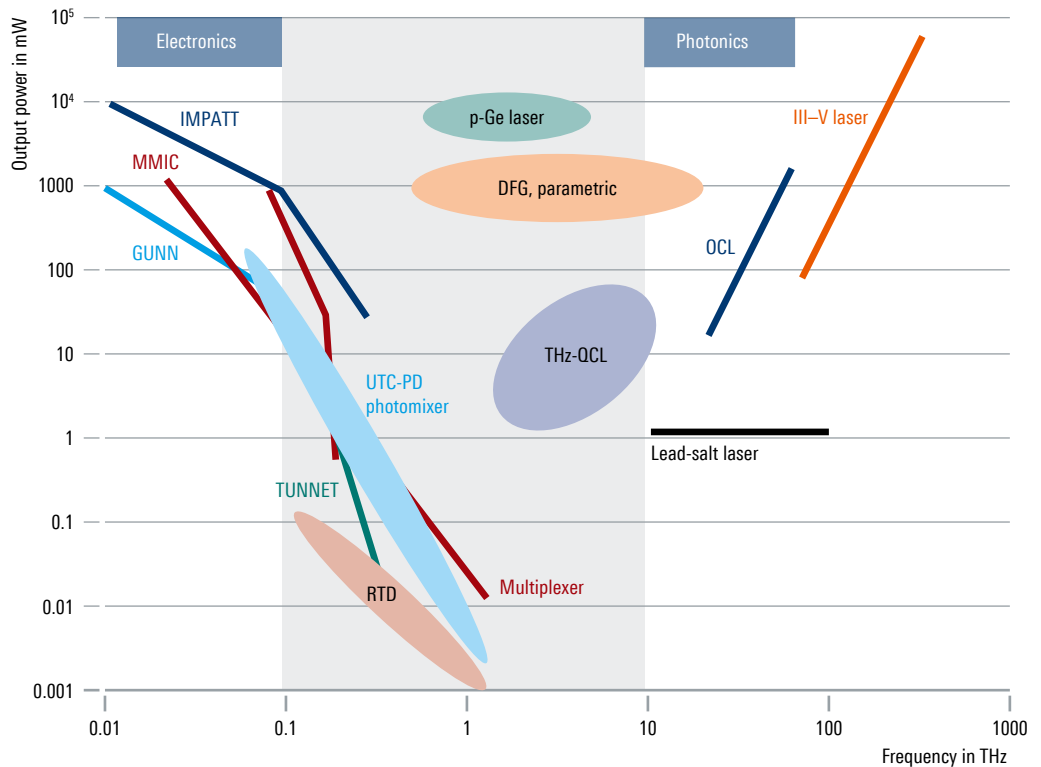
4.3   Sources for THz radiation on the borderline between electronics and photonics

There are three major approaches for generating terahertz (THz) radiation (Figure 10). Some examples will be described in more detail in the following sections.

Electronic sources

The "classic" approach using electronic sources has evolved tremendously in the past years, especially with the refinement of various semiconductor material components (see Chapter 5).

These sources include frequency multiplier chains ("upconversion"), resonant tunneling diodes (RTD), transistors and diodes. The advantage is that the components are very compact and can be operated at room temperature, but they have certain limitations in bandwidth and efficiency. However, electronic sources become comparably inefficient at terahertz frequencies and provide rather limited frequency tuning.

Direct generation: QCL

Direct THz generation with optical sources includes the very elegant quantum cascade laser (QCL) approach, nonlinear optics (parametric optical processes) and molecular lasers (inefficient and bulky). Quite reasonable power levels could already be reached with QCL, but the efficiency is still limited and often they must operate at cryogenic temperatures.

Indirect generation: Optoelectronics

In recent years, frequencies between 0.5 THz and 10 THz have also become the domain of laser based techniques. Optoelectronic (photonic) approaches use either tunable diode lasers or femtosecond lasers. Photomixers, photoconductive switches or nonlinear crystals convert the near-infrared laser light into terahertz waves, either spectrally resolved or broadband.

One particular approach that has gained increasing interest over the past years is "downconversion" from the optical frequency regime using ultrafast photodiodes and photoconductors. The main advantage is the tunability over a large range, operation at room temperature and the possibility to reuse mature technologies developed for fiber-optic communications. The power envelope has been pushed considerably, but there are still limitations in efficiency.

Figure 10: The three major approaches for THz radiation generation

Note that the energy equivalent of 1 THz corresponds to 49 K, necessitating the use of cryogenic cooling for certain technologies (e.g. QCL) due to relaxation processes at higher temperatures.
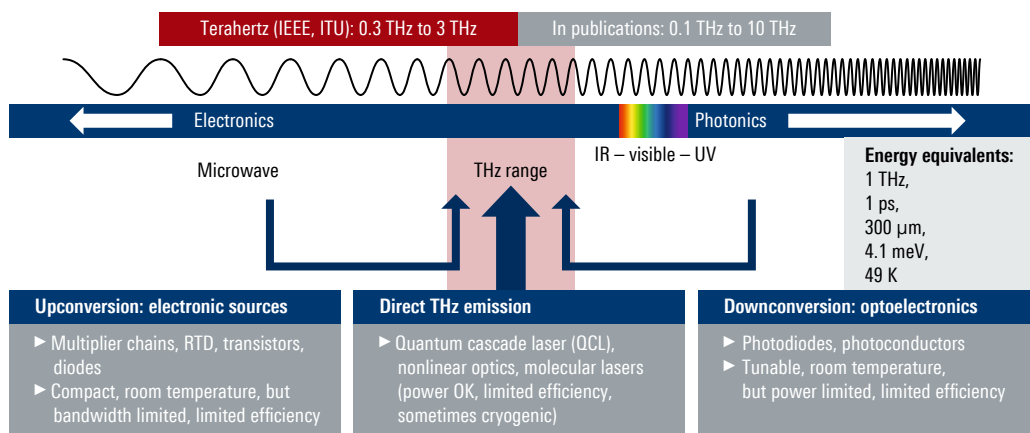
4.4 Upconversion: electronic THz wave generation and analysis

Since the founding of Rohde & Schwarz in 1933, the company's core competency has been in the development and manufacturing of advanced RF test and measurement equipment for all relevant electronic and microelectronic areas.

In order to support the multitude of 6G research activities including semiconductor industry research for device and circuit characterization in the millimeterwave and THz region, Rohde & Schwarz offers a broad range of development and analysis measurement tools. Some examples are given in the following sections:

▶ Vector network analyzer device characterization with frequency converters up to 1.1 THz
▶ Extended frequency range support for signal and spectrum analyzers via external harmonic mixers for e.g. the D band (110 GHz to 170 GHz) and other frequency bands up to 500 GHz (R&S®FS-Zxx series)
▶ Extended frequency range support for signal generators using frequency multipliers up to 170 GHz (R&S®SMZ series)
▶ Signal generation and analysis with transmit and receive converters for the D band spectrum (110 GHz to 170 GHz)
▶ Antenna radiation performance measurements in the D band (110 GHz to 170 GHz) using anechoic chambers

4.4.1 Vector network analyzer THz measurements with metrology-level accuracy

Vector network analyzers (VNA) that perform measurements in the mmWave and terahertz ranges are more in demand than ever. In the E band (60 GHz to 90 GHz), they are used, among other applications, to characterize active and passive components in wafer prober systems and waveguide assemblies. Even at higher frequencies, network analyzers can be used in a broad range of applications for testing integrated circuits, sensors and antennas, imaging systems, radio astronomy systems and materials. The 5G wireless communications standard and the production of automotive radar sensors have also created significant testing demand.

While measurements at frequencies of several GHz up to 67 GHz are part of the standard repertoire of network analyzers, tests in the mmWave and terahertz ranges are significantly more demanding as they require external frequency converters (which can cover up to 1.1 THz with the R&S®ZC1100). These frequency extenders upconvert stimulus signals and downconvert response signals to characterize devices that operate at frequencies in the terahertz range.

On-wafer characterization of active components

Characterizing active components in linear and nonlinear ranges requires defined input power at the probe tip. Since on-wafer power calibration is not possible, the power at the waveguide output is calibrated, and losses in additional waveguides, 1 mm cables and the probe tip are taken into account in the calibration process. For power sweeps and compression point measurements, the R&S®ZNA has an integrated calibration routine that is able to compensate for mmWave converter nonlinearities for maximum measurement dynamic range and reproducibility. The measurements commonly performed on active components at lower frequencies can be carried out with the R&S®ZNA just as conveniently at high frequencies using system-integrated mmWave converters at metrology-level precision [35].

Figure 11: Measurements in the terahertz range

With the R&S®ZNA vector network analyzer, measurements in the terahertz range using mmWave converters are configured just as conveniently as in lower frequency ranges (left). The MPI TS150-THZ integrated probe system with microscope configured with the R&S®ZNA for wafer-level measurements up to 330 GHz with GGB Industries Inc. waveguide probes directly mounted at the output of the mmWave R&S®ZC330 converters (right).

To demonstrate system capabilities, a four-stage 325 GHz MMIC low-noise amplifier (LNA) developed by the Fraunhofer Institute for Applied Solid State Physics IAF was measured (see Figure 12). The scalar gain $|S_{21}|$ is shown with the ±95 % confidence intervals.

Figure 12: Fraunhofer IAF four-stage, 325 GHz MMIC LNA (left) and measured scalar gain $|S_{21}|$ with the ±95 % confidence intervals (right) [35]
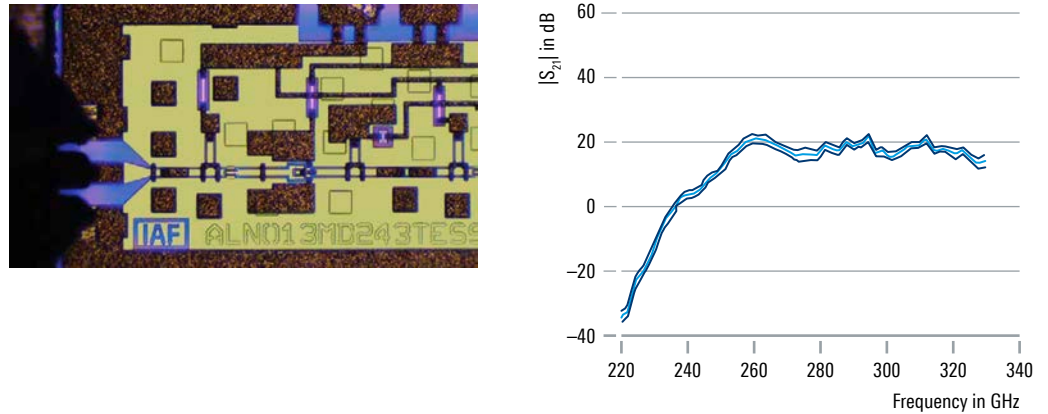
4.4.2 Wideband signal generation and analysis in the D band

Extending the carrier frequencies beyond 100 GHz, one of the focus frequency bands of 6G research lies in the D band (110 GHz to 170 GHz) due to the prospect of using much wider bandwidths of several GHz for the highest data rates. Figure 13 shows a test and measurement setup to support research for components and transceivers in this frequency region.

Figure 13: D band (110 GHz to 170 GHz) signal generation and analysis test setup with R&S®FE170ST frontend (transmitter, TX) and R&S®FE170SR frontend (receiver, RX)

In this sample setup, the TX and RX are directly connected with an attenuator.

Shown on the left is the R&S®FE170ST transmitter (TX) frontend which upconverts the modulated signals (e.g. potential 6G waveforms) from the R&S®SMW200A vector signal generator to the frequency range of 110 GHz to 170 GHz. On the right is the counterpart: the R&S®FE170SR receiver (RX) frontend which downconverts the signals and transmits the intermediate frequency (IF) to the R&S®FSW signal and spectrum analyzer. The demodulated signal exhibits excellent EVM performance underlining the extremely low phase noise of the generated signal.

MMIC design

The following pictures show two sample MMICs designed by Rohde & Schwarz and cooperation partners that are used in T&M equipment.

Figure 14: 27 GHz to 41 GHz GaN/SiC MMIC amplifier in proprietary SMT compatible package (left); 40 GHz to 70 GHz GaN/SiC MMIC amplifier (right)
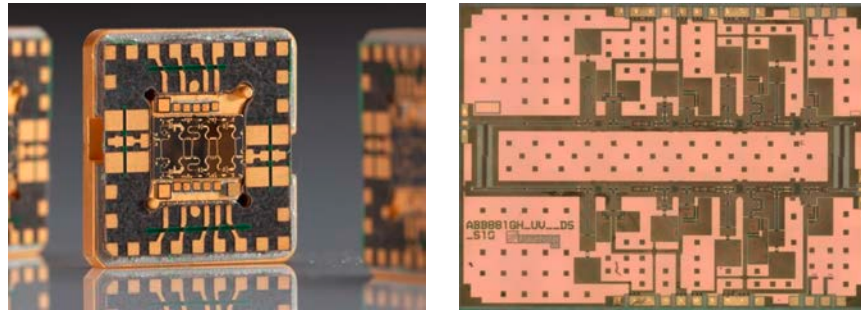
The 40 GHz to 70 GHz amplifier that is shown with dimensions of approx. 4 mm × 3 mm reflects the typical size of such circuits as used in the latest R&S®SMA100B analog signal generator from Rohde & Schwarz. This instrument offers the highest commercially available output power in the microwave range.

As another example, THz sources have also been developed by Radiometer Physics GmbH (RPG) with a combination of high-power amplifier GaAs MMICs up to the W band and high-power, high frequency multipliers based on GaAs Schottky diode MMICs. Figure 15 shows an example of such a frequency tunable source up to 1100 GHz for the heterodyne instrument for the far infrared (HIFI) onboard the Herschel space telescope (left) [36], covering the spectral range from far-infrared to submillimeter wavelengths. The picture on the right shows a frequency and power agile source up to 158 GHz for the submillimeterwave instrument (SWI) onboard the JUICE satellite from ESA (European Space Agency) [30].

Figure 15: RPG local oscillators for heterodyne receivers in the HIFI instrument

Onboard the Herschel space observatory (left) [36] and for the submillimeterwave instrument (SWI) onboard the ESA JUICE planetary mission [30] (left: RPG, Herschel/HIFI local oscillators, 480 GHz to 1100 GHz; right: RPG, JUICE/SWI local oscillator, 136 GHz to 158 GHz).
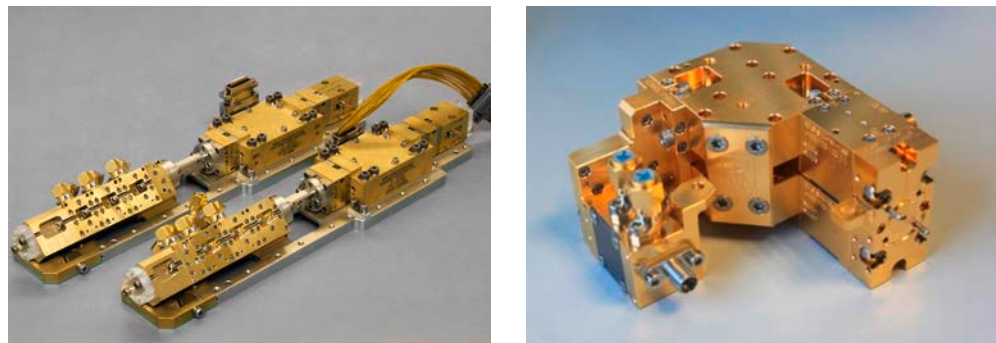
4.4.3 Antenna radiation performance measurements in the D band

5G pioneered the use of millimeterwave frequencies for wireless communications in connection with the development of over-the-air (OTA) testing concepts. This is due to the fact that large-scale and highly miniaturized antenna arrays are no longer accessible for conducted testing [37]. OTA antenna test concepts can be extended into the D band and beyond for exploring THz communications and sensing. Future devices will incorporate even more highly integrated active antenna systems for ultra-massive MIMO and sensing

applications. However, OTA testing will also be of interest in order to investigate the characteristics of reconfigurable intelligent surfaces (RIS).

Over-the-air testing (OTA) with the R&S®ATS1000

Research towards 6G is now putting the focus on frequencies above 100 GHz. There, the significant available spectrum is the key to enable much higher data rates. In this context, not only new wideband high-gain antenna concepts are needed but also advances in applied antenna measurement procedures.

Moving from legacy sub6 GHz cellular services to 5G NR frequency range 2 (FR2) was already a major technological leap (Figure 2). Since path loss increases with the square of frequency, higher gain antennas with electronic beamsteering capabilities were introduced in the user equipment and network infrastructure in order to ensure appropriate quality for the radio links. Due to the dramatic increase in the complexity of integrated circuits as a function of frequency, a majority of developments are now targeting a new incremental step at waveguide D band (110 GHz to 170 GHz) and G band (140 GHz to 220 GHz).

In the following discussion, we consider a spherical scanning solution for measuring radiation performance in the D band with the unprecedented dynamic range that is realized in the R&S®ATS1000 chamber. The solution uses a new probe design with direct downconversion that provides a dynamic range of greater than 50 dB at 170 GHz.

The R&S®ATS1000 simplifies the test requirements because no mechanical modification or additional RF cabling is needed to measure the amplitude and phase coherent response of a DUT in the frequency range from 110 GHz to 170 GHz.

Figure 16: D band leaky-wave fed lens antenna by IMST [38]
Simulated E-field distribution inside and outside the lens at 140 GHz (left). Schematic of the lens (center) and photo of the setup in the R&S®ATS1000 chamber (right).
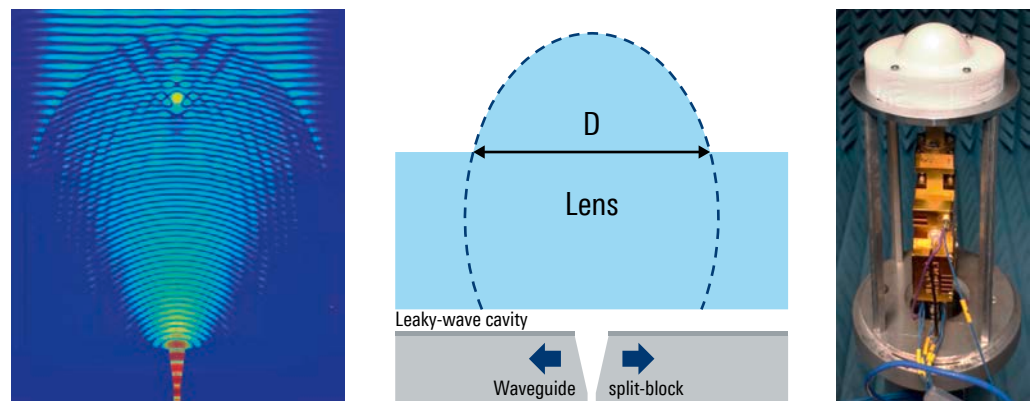
The device under test (DUT) is a newly designed D band lens based leaky-wave fed antenna by IMST (Figure 16). It could be used in 6G fronthaul point-to-multipoint scenarios. The simplified feeding structure consists of an elliptical lens made of low permittivity $\varepsilon_r = 2.34$ and low-loss high density polyethylene (HPDE) with 35 mm diameter (20λ at 170 GHz) which enables a cost-effective design. The feed consists of a λ/2 leaky-wave air cavity, excited by a WR6 waveguide. The radiation pattern can be steered by displacing the feeder along the lens focal plane.

This antenna was both modeled numerically and evaluated experimentally with a compact system using spherical near field scanning. The radiation pattern measurements

were carried out in the R&S®ATS1000 mobile spherical scanning range (Figure 17). This fully anechoic chamber includes a distributed axis positioner.

A DUT feeding assembly is used to perform phase coherent and time stable measurements. It is shown below the lens antenna in Figure 17. This chain consists of a D band subharmonic mixer, identical to the one that is used at the probe, and a D band isolator that is attached to the WR6 split-block of the DUT. Measurements are performed with the R&S®ZNA43 4-port vector network analyzer (VNA) where one port at the front feeds the IF signal to the DUT.

Figure 17: Measurement setup using a compact spherical scanning system with frequency converted probe and DUT at the azimuth pole

Block diagram of the frequency converted probe concept (inset)

Figure 17 (inset) shows the measurement probe concept. An orthomode transducer (OMT) is connected to a 20 dBi squared horn antenna with a 3 dB beamwidth of 16° and a cross-polarization isolation of 25 dB over the complete D band frequency range. The assembly works reciprocally and is able to transmit or receive two orthogonally-polarized fields when the DUT is set to receive (RX) or transmit (TX). Downconversion or upconversion is realized directly at the probe, thereby removing any cable loss at RF frequencies. Both polarizations can be measured simultaneously.

Figure 18: E-plane and H-plane

Simulated, measured and near field to far field (NF2FF) transformed normalized directivity patterns as a function of frequency for boresight (direction of maximum gain) radiation.
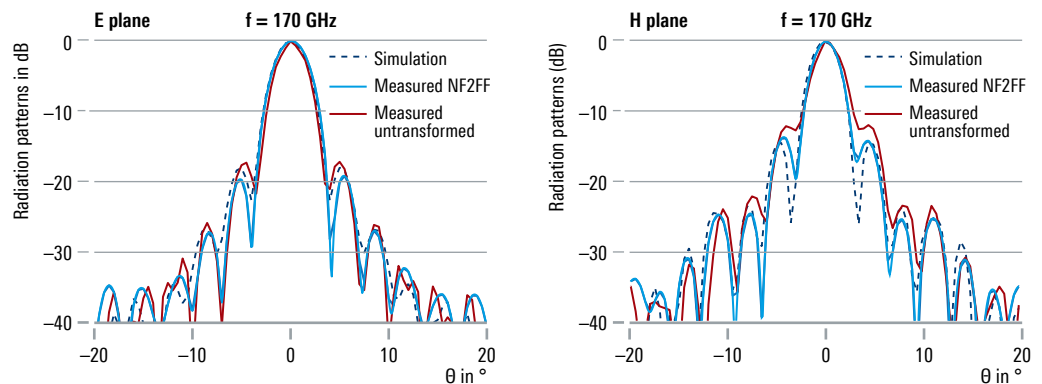
The results in Figure 18 reveal excellent agreement between the DUT full-wave simulations and the measurements. This confirms the high accuracy of the measurement system and technique involving the new probe design. Phase coherent data acquisition such as near field to far field (NF2FF) transformation can be successfully realized for passive antenna measurements. Interestingly, the untransformed measurement results in red show that the main beam of the radiation pattern is already close to far field asymptotic behavior.

In conclusion, a high efficiency D band lens antenna design was presented with realized gain greater than 30 dB over 42 % bandwidth. Accurate characterization of this antenna was performed with a spherical scanning test system, capable of stable phase coherent measurements, with direct frequency conversion at the DUT input and at the test probe outputs. Phase coherence is a must to support precise application of the near field to far field transformation algorithms that are essential for accurate determination of radiation pattern nulls and sidelobe levels.

4.5 Direct THz photon generation: quantum cascade laser (QCL)

4.5.1 Interband diode laser

Optical versus THz frequencies: interband versus intraband transition

Generation of phase coherent radiation in a laser (light amplification by stimulated emission of radiation) has been an established concept for many years. It has led to many applications, among them optical communications in conjunction with optical fiber technology, the technical foundation of today's internet. A laser consists of an active medium (with the laser transition between energy levels with population inversion), a cavity for feedback and additional frequency selective components.

Interband diode laser

Semiconductor laser diodes are among the most important optoelectronic components as they allow direct conversion of electrical current into coherent light. For optoelectronics, the direct bandgap III–V semiconductor materials GaAs and GaN are most important. The recombination of an electron (e$^-$) from the conduction band with a hole (e$^+$) from the valence band leads to the emission of a photon with a frequency corresponding to the difference between the energy levels (Figure 19). Interband diode lasers are cheap and efficient for generating photons from ultraviolet across visible light to the IR frequency region. However, THz photons have energies 100 times to 1000 times smaller than visible photons and there are no materials with such a small bandgap and population inversion.

Figure 19: Interband diode laser versus quantum cascade laser (QCL)

Whereas in an interband diode laser the laser transition between the excited state energy level $|e\rangle$ and the ground state $|g\rangle$ occurs between the conduction band and the valence band, in a QCL the photon transition occurs between designed quantum well energy levels ("wavefunction engineering") within the conduction band $h\nu$.
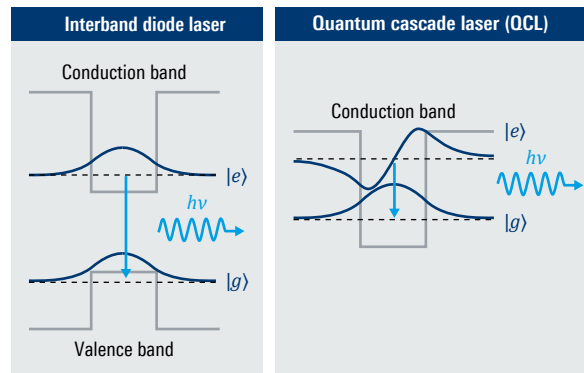
4.5.2 THz QCL: Lasing transition between intersubbands engineered by heterostructures

In contrast to the interband diode laser, laser emission is achieved in a QCL through the use of intersubband transitions in a periodic stack of semiconductor multiple quantum well heterostructures ("superlattice"; Figure 19). The concept was first demonstrated in 1994 by a research group at Bell Labs by Jérôme Faist et al [39].

Figure 20 shows an illustration of the periodic quantum well heterostructure (epitaxially grown GaAs or InP structures with a thickness of a few nm) and the resulting quantum well energy level structure. The well depths can be engineered by controlling the layer depths during the fabrication process. Hence, the wavelength of the lasing transition is dependent on the physical structure of the device ("electron wavefunction engineering"). This concept allows generation of low energy THz photons not accessible with interband diode lasers.

Operating principle (Figure 20): Photons of frequency ν are emitted via intersubband transitions of electrons from the excited state $|e\rangle$ to the ground state $|g\rangle$, where $E = h\nu$ is the energy difference between the ground and excited states. One advantage of the concept is that the electron responsible for the emission of the photon tunnels into the next quantum well (active region) with subsequent emission of a photon. As a result, multiple photons can be generated by a single electron, thereby making the process extremely efficient. The tunneling from one well to the next is where the term "quantum cascade" originates from.

Figure 20: QCL: Lasing transition between intersubbands engineered by semiconductor heterostructures
"Band structure and electron waveform engineering": Light is emitted as electrons "cascade" through multiple quantum wells forming a "superlattice".
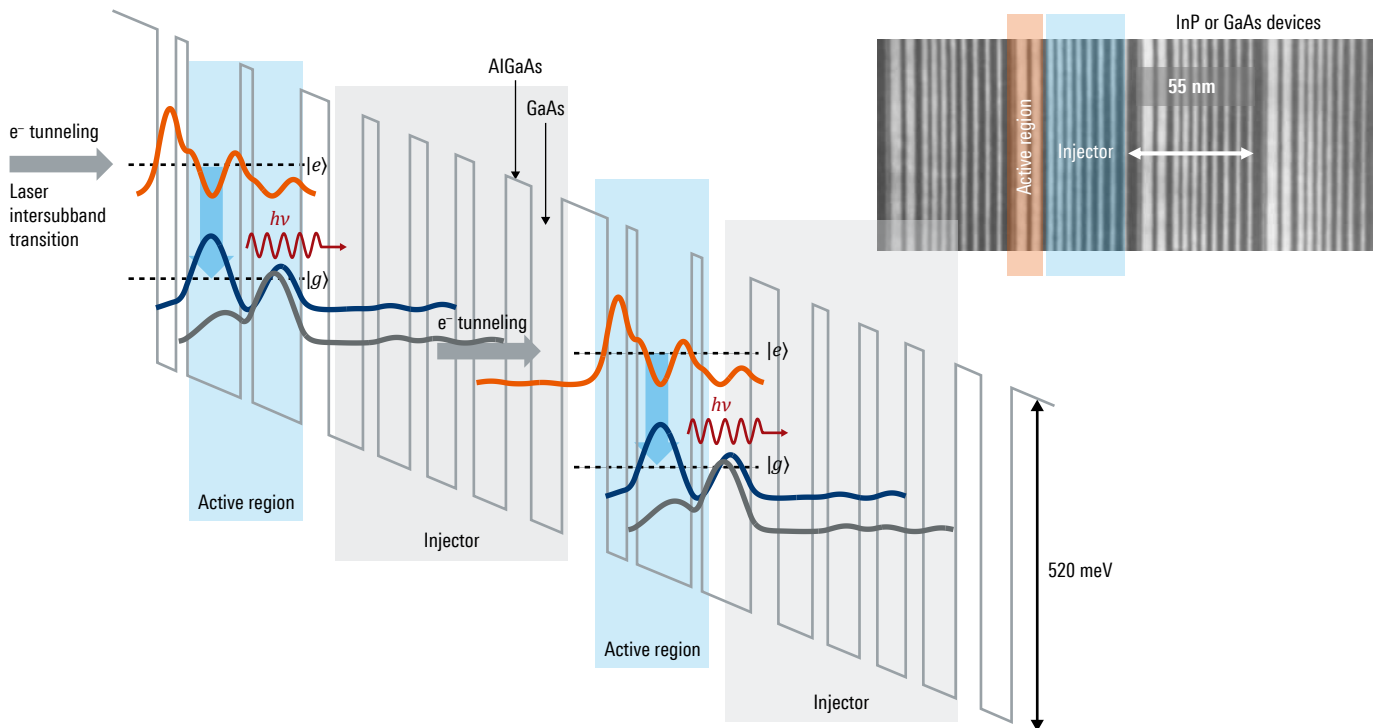
For reference, the optical wavelength of 850 nm corresponds to an energy difference of 1.4 eV.

Successful operation of a QCL at THz frequencies was first demonstrated in 2002 [40]. Since then, QCLs have quickly progressed in terms of frequency coverage, increased power output and increased operating temperature. By carefully designing the quantum wells, lasing has been achieved at wavelengths as short as 2.75 µm (109 THz) and as long as 161 µm (1.9 THz). The longer wavelength devices still require cryogenic cooling, but room temperature operation has been observed to at least 16 µm. Interest has been concentrated in the mid-infrared (3.5 µm to 13 µm) and terahertz spectrum (2 THz to 5 THz ≈ 60 µm to 150 µm). An approach using long-wavelength THz QCL sources with intra-cavity nonlinear frequency mixing has even made frequencies below 1 THz accessible [41].

The journey towards realizing a terahertz quantum cascade laser that operates at room temperature has taken a step forward with the recent publication of a device that operates at –23 °C, within the reach of Peltier coolers [42].

4.6 Downconversion photonic approach: from optical to THz via photomixing

Optoelectronic frequency domain THz generation: uni-traveling carrier photodiode (UTC-PD) and PIN photodiode as photomixer

An indirect approach for continuous wave THz generation has recently attracted strong interest: A photodiode can efficiently convert an optical signal into an electrical signal by optical heterodyning in high bandwidth photoconductors via a "photomixing" process. It involves optical/infrared laser light generating free charge carriers in a semiconductor or organic crystal. The charge carriers are accelerated by internal or external electric fields and the resulting photocurrent becomes the source of the terahertz wave.

As depicted in Figure 21, in this approach the output of two continuous wave (CW) single-mode lasers (often at the 1.55 µm "fiber telecom wavelength") with closely spaced emission frequencies at ν_1 and ν_2, respectively, are "mixed" in an ultrafast III–V compound semiconductor photodetector (InGaAs/InP), inducing a photocurrent modulated at the optical beat frequency $\nu_{THz} = \nu_1 - \nu_2$ in the THz region. An antenna structure surrounding the photomixer translates the oscillating photocurrent into the terahertz wave. State-of-the-art photomixers are based on either GaAs or InGaAs/InP and require laser wavelengths below the semiconductor bandgap (i.e. around 0.8 µm or 1.5 µm, respectively).

The photomixing technique has the advantage that by tuning the lasers, the difference frequency of the beat note can be varied over a broad spectral range, which translates directly into widely tunable THz radiation [43] [44].

Figure 21: Photomixing process

Photomixing process to generate THz radiation at the beat frequency $\nu_{THz} = \nu_1 - \nu_2$ of two slightly detuned single-mode lasers. One way to attain extreme frequency and phase stability is to derive both frequencies from an optical frequency comb. For data transmission, one of the lasers is modulated by a Mach-Zehnder modulator (MZM): It consists of an interferometer where the beam is split into two. In one of the interferometer arms, the phase of the laser light is shifted relative to the other path by an electro-optic modulator (EOM), resulting in a constructively or destructively modulated laser beam after recombination of both beams. The beat signal impinges the photomixer uni-traveling carrier photodiode (UTC-PD) and the integrated antenna emits THz radiation.
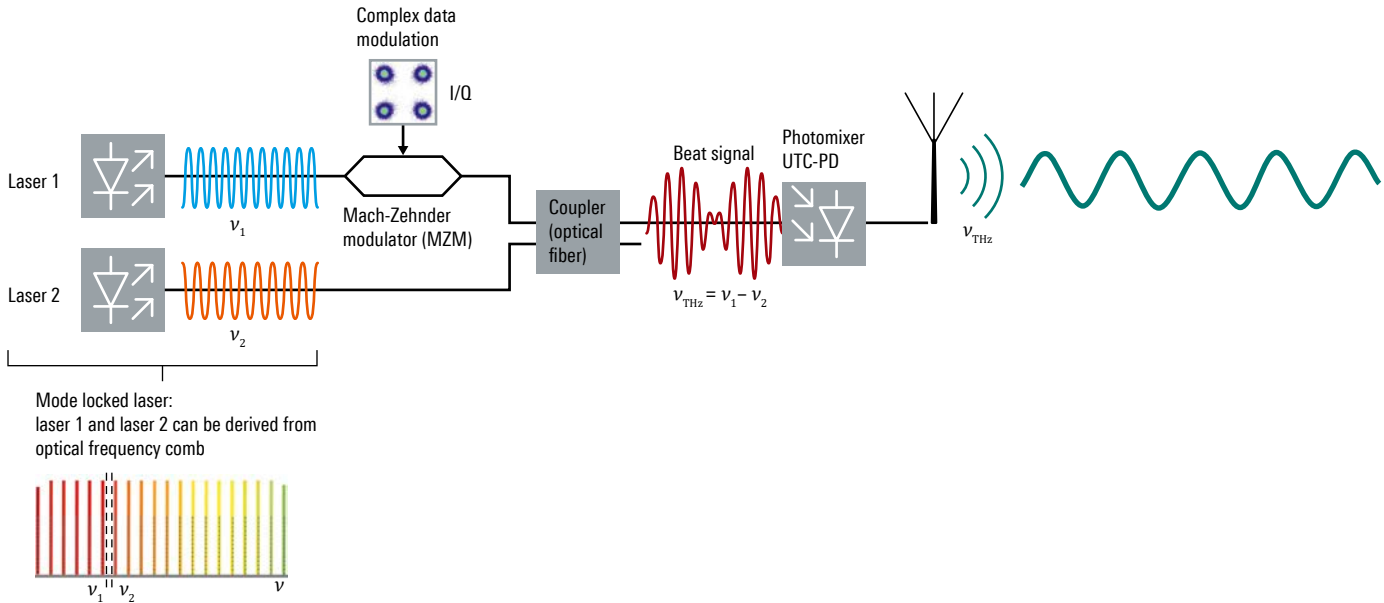
Two types of photodiodes are commonly used: PIN photodiodes (PIN-PD) and uni-traveling carrier photodiodes (UTC-PD) [45]. Both types were originally developed as detectors for fiber-optical communications networks, but later modified to match the requirements of THz emission. UTC-PDs were originally developed by NTT in Japan for multi-stage optical reception at 40 Gbps, but these photodiodes have been enhanced to enable generation of signals up to 4.5 THz [46] [47].

In the frequency bands suitable for communications applications such as the 300 GHz band, power levels on the order of mW have been achieved [48] [49].

The combination of the tunable feature of the laser beams with the photomixing technique allows transfer of the techniques for generating optical vector fields developed for optical communications (e.g. with Mach-Zehnder modulators with modulation bandwidths > 100 Gbps) and thus technological advancement into the THz range. Furthermore, if extra frequencies are added, these techniques make it relatively easy to implement multi-frequency communications (Figure 21). The combination also allows easy integration of these wireless links into fiber-optic infrastructure. Furthermore, on-chip communications and future high speed inter-device communications will also require THz waveguides. Such waveguides have recently been realized utilizing topological valley photonic crystals exhibiting near zero bending loss and zero backscattering [50]. As shown in Figure 21, referencing both frequencies to the same frequency comb generator allows transfer of the unique phase and frequency stability of optical combs in a broadband and tunable manner into the THz range [51] [52]. The receiver side, corresponding to the transmitter shown in Figure 21, could be a Schottky diode or a setup that is symmetrical to the transmitter side. This technology also holds promise for T&M instruments since it can be scaled up to extend the spectrum analysis and vector network analysis frequency range via optoelectronics into the THz region [53] [54].

THz waves for communications: 300 GHz point-to-point transmission

Figure 22 shows examples of THz data transmission trials (SISO, i.e. with one transmit antenna and one receive antenna) performed in the lab and outdoors. Between 200 GHz and 300 GHz, there is a transmission window with low atmospheric losses (Figure 7). In contrast to free-space optical links, millimeterwave or terahertz transmission is much less affected by adverse weather conditions like rain and fog. While the left side of Figure 22 shows examples of 100 Gbps in the lab, the right photo shows a transmission link at 300 GHz in the harbor of Dunkerque over a distance of 850 m (with a very focused beam).

On the left side of Figure 22, an UTC-PD InGaAs/InP chip fabricated at IEMN is shown with the response curve photodiode output versus photo current (credit: IEMN UMR CNRS 8520/University of Lille-Renatech Network, France) [55]. This photodiode is using a semitransparent top contact with subwavelength apertures for enhanced optical transmission, front-side illumination of the photodiode (1.55 µm wavelength). The responsivity of the device is further increased by using a metallic mirror below the diode mesa through wafer bonding.

Further demonstrations of 100 Gbps transmission in the terahertz window between 200 GHz and 300 GHz have been realized [56] [57] [58] [59].

Figure 22: Examples of data transmission around 300 GHz in the lab (left) [55] and an outdoor trial (right)

A 300 GHz link with live HD video transmission was established in the harbor of Dunkerque over a distance of 850 m where very good directional alignment is crucial (courtesy of Prof. G. Ducournau, IEMN, CNRS-Université de Lille).
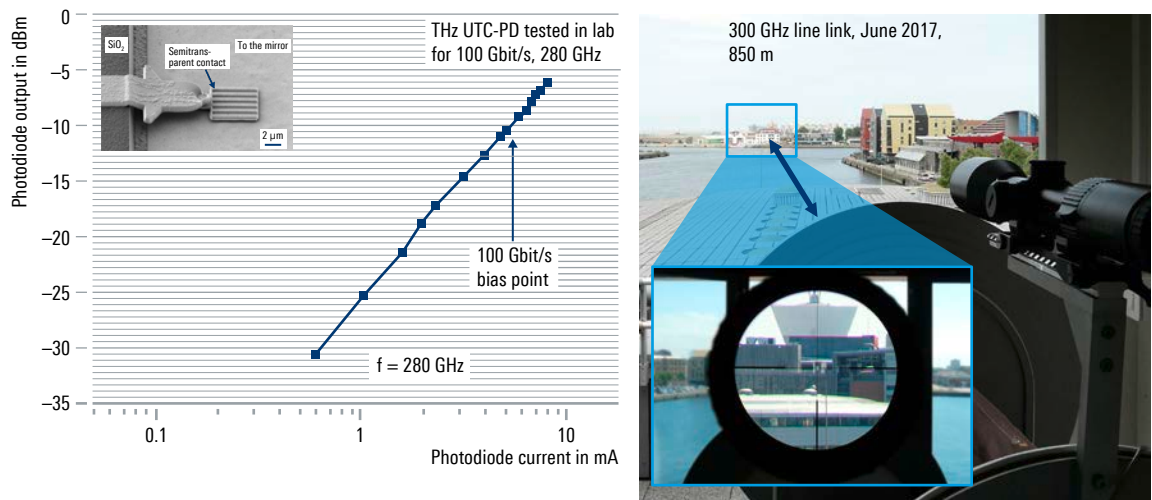
4.7 Time domain THz generation: Spectroscopy and imaging based on a femtosecond laser

Another alternative approach to cover very large frequency ranges (i.e. 0.1 THz to 6 THz) involves time domain (TD) systems which are used for spectroscopy (TDS) and imaging. In such a setup, pulsed terahertz radiation is generated via femtosecond lasers. The laser pulse is split into two parts with a beam splitter: One part travels to the THz transmitter, the other part to the detector. The ultrashort laser pulse produces a transient current in the emitter, a photoconductive antenna, resulting in an electromagnetic wave packet with a broad spectrum in the terahertz range [60] [61].

The terahertz pulse interacts with the spectroscopy sample and reaches the receiver, which works in a "pump and probe" fashion: The incident terahertz pulse changes certain characteristic properties of the material (e.g. conductivity or birefringence) and the separated laser pulse probes this effect. A variable delay stage scans the terahertz wave packet with the much shorter "probe" pulse. A Fourier transform of the terahertz amplitude then reproduces the spectrum.

Time domain spectroscopy offers the advantage of a very large spectrum range and high measurement speed. Commercial systems generate spectra up to 6 THz. Terahertz time domain systems are used in a variety of industrial applications such as nondestructive testing in quality assurance [25], in particular for synthetic materials such as polymers and ceramics. From the terahertz measurements, the complex refraction index (permittivity) and geometrical structures can be derived. One application example is thickness gauging via time of flight measurements which is used, for example, in paper production: The broad spectrum translates into micrometer-level thickness resolution.

Figure 23 shows a terahertz image of a prepaid card recorded by a time domain spectrometer (TeraFlash pro, TOPTICA Photonics AG). The sample was probed with frequencies from 100 GHz up to 6 THz.

Figure 23: Photograph (left) and processed terahertz image (right) of a Japanese prepaid public transport card, revealing an inside view of the underlying electronics (courtesy of TOPTICA Photonics AG)

5 SEMICONDUCTOR TECHNOLOGIES FOR mmWAVE AND THz ELECTRONICS

Modern society's growing demand for wireless connectivity with higher data rates as well as radar imaging systems with higher resolution is driving a continuous increase in the frequencies at which these microwave systems operate. While 5G has set the stage for utilizing mmWave frequencies for wireless communications networks, research into 6G as well as satellite communications links is further propelling the development of mmWave systems into the range beyond 100 GHz.

This trend poses an increasing challenge for the semiconductor industry to provide components to deliver high output power at extremely high frequencies. Power amplifiers, often realized as monolithic microwave integrated circuits (MMIC), are among the most essential components of wireless communications and imaging systems. They have a decisive influence on the overall system's performance in terms of output power, efficiency, bandwidth, linearity and noise.

Here, we highlight some key properties of the relevant semiconductor materials for high frequency applications along with the development status of state-of-the-art power amplifiers.

5.1 Material properties of semiconductors for high frequency applications

High power at high frequencies: III–V semiconductors (GaAs, GaN, InP) versus silicon (SiGe)
While III–V semiconductors with their direct bandgap are the ideal material for optoelectronics (lasers) and high frequency applications, silicon technology has the most advanced large-scale manufacturing processes enabling cost-efficient solutions for commercial applications.

The different high speed semiconductor material properties are summarized and compared in the radar plot below (Figure 24).

Figure 24: Comparison of selected material properties of mmWave semiconductors [62]
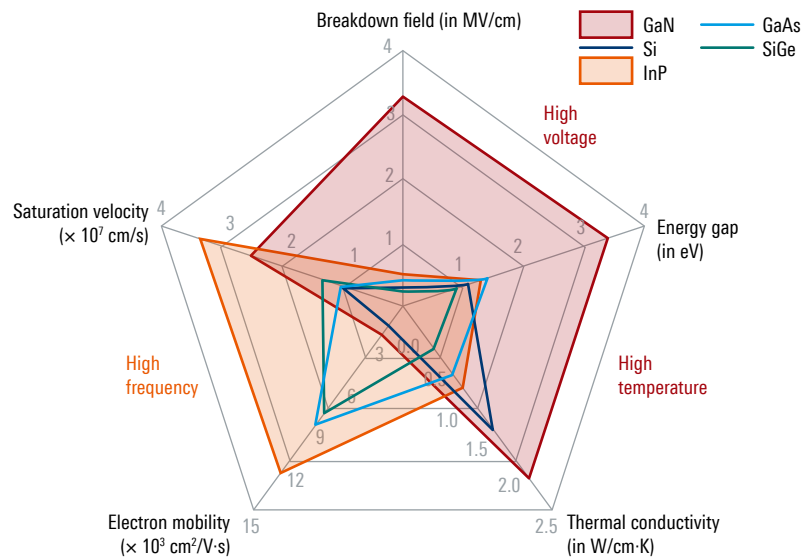
We provide a brief description of the key parameters below:

Electron mobility

The ability of a charge carrier to move and follow according to the applied E-field is referred to as mobility. Since electrons exhibit higher mobility than positively charged holes, high speed semiconductor devices are all based on electron transfer currents. For this reason, the parameter "electron mobility" is relevant. This parameter has the unit [m²/(Vs)].

Saturation velocity

This parameter describes the maximum speed of an electron in a semiconductor device when the charge is driven by high E-field strengths. The unit of the parameter is simply that of velocity [m/s]. The operating state of a device operated at high field strength is also called "velocity saturation".

Breakdown field strength

The parameter with the unit [V/m] describes the ability of a material to withstand high voltages before it becomes conductive (which is usually destructive for the device in the absence of current limitation). The maximum operating voltage of the device is strongly defined by this parameter. There are techniques, like the application of field plates, to improve and equalize the field strength distribution in a semiconductor device to increase its breakdown voltage.

Energy gap

The energy gap or bandgap is measured in [eV] and is a quantum physics based property describing the energy difference between the conduction and valence band where no energy states are available in an undoped semiconductor. For heterojunction devices, the bandgap structure is shaped by adding additional materials to the semiconductor alloy to improve device performance (e.g. SiGe HBTs or III/V based HEMT devices).

Thermal conductivity

This parameter describes the ability of a substrate material to conduct thermal energy and is measured in [W/(mK)]. Especially for power applications like power amplifiers, this is an essential parameter since very often the device output power is thermally limited. This is especially true for GaN HEMTs which need to be operated far below their breakdown voltage for thermal reasons. Note that for this reason, high-end GaN devices are manufactured on lattice matched substrates exhibiting high thermal conductivity such as SiC or even diamond.

The degree to which the above parameters are more or less pronounced in a given semiconductor material strongly impacts its application fields.

Gallium arsenide (GaAs)

GaAs has a relatively high electron mobility and saturation velocity (Figure 24) depending on the doping concentration. Thus, extremely high frequencies can be achieved. The material cost is high, but there exists a great deal of industry heritage.

GaAs technologies are available nowadays for Schottky diodes, pseudomorphic high electron mobility transistors (pHEMT) and heterojunction bipolar transistors (HBT). GaAs pHEMT technology exhibits good broadband noise up to high frequencies. HBTs are especially well suited in cases where low 1/f noise is desirable in combination with high breakdown voltages. GaAs Schottky diodes can be used to produce very low-noise receivers up to 4.7 THz. It can also be used for high efficiency multiplication up to several THz, making it a very versatile millimeterwave technology.

GaAs mixer and multiplier devices can either be integrated as an MMIC into a module, or flip-chip transferred onto host substrates to improve dielectric loading and/or thermal dissipation.

Indium phosphide (InP)

InP has the highest electron mobility and saturation velocity. Thus, extremely high frequencies can be achieved. However, the material cost is high and wafer/chip handling is difficult.

InP technologies are available in the form of heterojunction bipolar transistors (HBT) and high electron mobility transistors (HEMT). The bipolar version is usually applied for analog integrated circuits where the speed and/or breakdown of state-of-the-art SiGe HBTs are insufficient. InP HEMTs have their domain in applications beyond 400 GHz and are used predominately for ultra-low-noise amplifiers at frequencies up to 700 GHz.

From an application point of view, indium gallium arsenide (InGaAs) metamorphic HEMT (mHEMT) technologies are comparable to InP HEMT technologies except that they use GaAs substrates.

Gallium nitride (GaN)

GaN received considerable attention when it was shown to enable realization of blue LEDs (InGaN) and subsequently, blue lasers. This lead to a Nobel prize in physics in 2014 [63]. GaN also provides certain favorable material features for high-power applications, namely a high energy gap, a high breakdown field strength and in combination with silicon carbide (SiC) substrates, good thermal conductivity for heat dissipation. This allows GaN transistors to operate under high bias voltages and thus deliver high output power. The lack of mature bulk GaN source material and the insufficient thermal conductivity of GaN led to the need for growing GaN heterostructures on carrier substrates such as silicon carbide (SiC), Si and lately even diamond. SiC is the mainstream substrate material for high-power, high frequency applications owing to its excellent thermal conductivity and low lattice mismatch to GaN. GaN on Si is a more cost-effective solution that makes perfect sense for monolithic integration with CMOS. Si substrates exhibit significantly higher dielectric losses compared to SiC, which makes a significant difference for millimeterwave MMICs. Furthermore, the thermal conductivity at room temperature differs by a factor of three in favor of SiC (400 W/(m·K) versus 130 W/(m·K)). Since the safe operating area of GaN HEMT transistors is limited by thermal boundary conditions, the substrate's thermal conductivity is of utmost importance in order to achieve high output power combined with a reasonable mean time to failure (MTTF).

Due to efficiency advantages and the possibility to operate at much higher channel temperatures, GaN has almost completely replaced silicon based LDMOS technologies for sub10 GHz base stations. It has also recently been used for microwave backhaul applications.

The above-mentioned high bandgap of GaN in combination with maximum channel temperatures up to +200°C makes the technology an excellent candidate for harsh environments. Especially spaceborne applications benefit from the radiation hardness of the technology due to the high bandgap and the ability to operate in a huge temperature range ("day and night"). Compared to other semiconductor technologies, GaN amplifier systems exhibit a very low mass to output power and volume to output power ratio.

Silicon germanium (SiGe) HBT and CMOS

SiGe heterojunction bipolar transistors (HBT) also offer comparably good electron mobility allowing their use for high speed analog applications. The full advantage of this technology can be exploited if combined with complementary metal oxide semiconductor (CMOS) technology to realize mixed signal ASICs containing high speed analog and digital functionality at a moderate cost. The combination of CMOS and SiGe HBTs is often referred to as "BiCMOS" processes. The prospect of utilizing mature CMOS manufacturing processes and combining high frequency components with analog/digital signal processing circuitry on the same die enables unprecedented levels of integration and flexibility.

SiGe HBTs on their own represent a widely used material for automotive radar applications or short-range communications. Here, the breakdown voltage of the technology is sufficient to provide the necessary output power. Recently, there has also been interest in this material for microwave backhauls in order to obtain lower production costs per chip with high volumes and high integration density.

Hetero-integration as a 6G research topic

Since there is not just one single semiconductor technology that is relevant for millimeterwave applications, a recent research area for 6G is hetero-integration of various semiconductor technologies to optimize performance and energy consumption, e.g. combinations of InP (speed), CMOS (integration density) and GaN (output power).

Table 2: Semiconductor materials with their corresponding properties and applications

Technology	Properties	Typical transistor types	Application
Si FET	▶ Material cheap, 8"/12" wafers ▶ Very high integration capability ▶ Low output power, medium speed for Si transistors ▶ Si substrate	▶ MOS/CMOS (FinFET configuration for small node sizes) ▶ Laterally diffused MOS (LDMOS)	▶ Digital (CPU, DSP) ▶ RF-CMOS (e.g. low power IoT devices) ▶ Sub-10 GHz power applications such as base station amplifiers
SiGe HBT	▶ Material cheap, 8"/12" wafers ▶ High integration capability ▶ Low output power, very high speed for SiGe transistors ▶ Si substrate	▶ Heterojunction bipolar transistors (HBT) ▶ CMOS and HBT	Analog high speed integrated circuits (amplifier, mixer, VCO, multiplier, divider, transceiver, etc.)
BiCMOS	▶ Material cheap, 8"/12" wafers ▶ High integration capability ▶ Mixed signal capability for most complex on-chip systems ▶ Si substrate	CMOS and HBT	Mixed signal devices (ADC, DAC, monolithic RF/analog/digital sub-systems in general, etc.)
GaAs	▶ Material expensive, 4"/6" wafers ▶ Low integration capability ▶ Medium output power, high speed ▶ GaAs substrate	▶ pHEMT	▶ RF blocks (amplifier, mixer, switches, etc.)
		▶ HBT (e.g. InGaP)	▶ Analog RF with good 1/f noise performance where breakdown voltage of SiGe is insufficient (e.g. VCO, mixer)
		▶ mHEMT	▶ Ultra-high-speed and low-noise LNA, comparable to InP HEMT
GaN	▶ Material expensive, needs different substrate since there are no GaN wafers, 4"/6" wafers ▶ Low integration capability ▶ Very high output power, medium speed ▶ SiC, Si or diamond substrate	HEMT	High-power applications (amplifier, switches)
InP	▶ Material expensive, 3"/4" wafers ▶ Low integration capability ▶ Medium output power, very high speed ▶ InP substrate	▶ HEMT ▶ HBT	▶ Ultra-high-speed and low-noise LNA, comparable to mHEMT ▶ Analog RF functions (amplifier, mixer, multiplier, divider, etc.) ▶ Alternative to SiGe HBT if higher speed and breakdown voltage can be traded against integration density

5.2 Overview of state-of-the-art mmWave power amplifiers

Applications that go beyond 5G and 6G are pushing the frequency boundaries. The relevant data points are "bunched" around the driving applications.

An overview of state-of-the-art mmWave amplifiers based on data collected in [64] [65] is shown in Figure 25. Each data point represents a measurement published in a paper over the years. The left side includes measurements up to 2016 whereas the right graph summarizes works until 2020.

Figure 25: Overview of state-of-the-art high frequency power amplifiers as of September 2016 (left) and October 2020 (right) [64] [65]
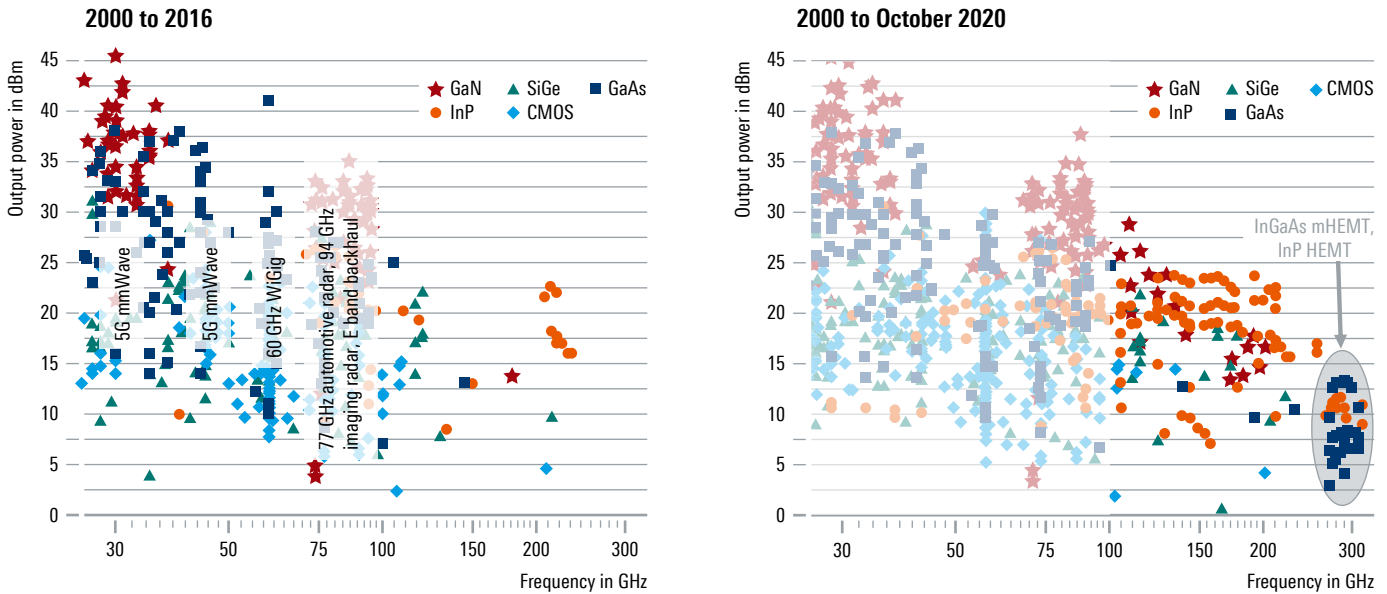
It is apparent that the data points (in different colors for different semiconductor technologies) are not equally distributed over the frequency range but rather are bunched around certain frequency bands. This is obviously due to the fact that the applications driving development are grouped around certain frequency allocations. For example, a large group of results was published around 28 GHz that is associated with the development of circuits for infrastructure and terminals for 5G New Radio (NR) mmWave bands such as n258 (24 GHz to 28 GHz), n257 (26 GHz to 30 GHz) and n260 (37 GHz to 40 GHz). Another group of results is concentrated around 60 GHz for WiGig with a large contribution of CMOS based circuits.

The last conglomeration of data points between 70 GHz and 95 GHz comprises a variety of applications. 77 GHz is used for automotive radar while some imaging radar systems operate around 94 GHz. Moreover, E band backhaul and point-to-point high data rate communications links are also found here.

It is interesting to note that before 2016, only a few results were published above 100 GHz. However, tremendous progress has been made in recent years among the higher mmWave bands. This is thanks to designs based on InP and to a lesser extent on SiGe and InGaAs mHEMT systems. The driver behind this progress is clearly the next generation of 6G communications.

The frequency envelope for power amplifiers has even been pushed beyond 300 GHz – albeit at lower power levels – to 500 GHz with a few milliwatts of power [66] [65] and up to 1 THz with sub-milliwatt power levels [67].

6 CHANNEL PROPAGATION MEASUREMENTS ABOVE 100 GHz

6.1 From channel sounding to channel models

mmWave and THz frequency propagation characteristics as the foundation for a new physical layer

The development of subterahertz communications as envisaged for 6G is only possible on the basis of a solid understanding of the properties of electromagnetic wave propagation in this as yet insufficiently researched frequency range.

This chapter explains the time domain channel sounding concept and presents exemplary results for a channel measurement campaign in the H/J band around 300 GHz and the D band (110 GHz to 170 GHz) in representative outdoor and indoor scenarios. This research activity aims to obtain a better understanding of the millimeterwave and submillimeterwave (sub-THz and THz) mobile radio channel also with respect to "the technical feasibility of IMT in-bands above 100 GHz" as currently discussed in the ITU-R WP5D [68].

Channel models as the basis for utilizing new frequency ranges

Before a new communications standard can be developed, the propagation properties in the designated frequency band must be understood and characterized. Then, channel models can be derived to enable system-level simulations of the new standard. Physical layer parameters include the distribution of pilot signals in the time-frequency domain which allow the receiver to equalize and compensate channel effects on the transmitted signal. Such characterization is needed to develop and verify coding and error correction schemes.

The underlying measurement data must correctly reproduce the investigated environment. Geometry based stochastic channel models (GSCM) such as 3GPP TR 38.901 [69], which is valid up to 100 GHz, are based on a large number of channel measurements in different environment scenarios.

3GPP channel model development and specification up to 4G was limited to the frequency range below 6 GHz and quasi-static environments. Dynamic scenarios and other types of environmental scenarios corresponding to new use cases, such as automotive, high speed trains and industrial environments, became relevant with 5G as the frequency range has been extended to the millimeterwave region. The resulting channel models, however, cannot simply be extended to the range above 100 GHz where 6G is intended to operate. They have to be verified and fine-tuned to correctly reflect the impact of the environment. Even more than in the millimeterwave range, propagation in this frequency range is strongly influenced by human bodies, vehicles and environmental conditions such as rain.

From channel sounding to channel models

Channel measurements by channel sounding deliver an image of the propagation properties of electromagnetic waves at a particular frequency. The term "channel sounding" comes from sonar technology, where short acoustic pulses are sent out from a ship or submarine and the reflections are recorded in the time domain [70]. This provides a viable image of the surroundings. With sonar, the transmitter and receiver are in the same place; with channel sounding for electromagnetic waves, the transmitter and receiver are spatially separated. In time domain channel sounding, a modulated pulse signal with excellent autocorrelation properties such as a Frank-Zadoff-Chu (FZC) sequence serves as a "ping" whose channel impulse response (CIR) is recorded. This propagation time measurement is very similar to the time delay measurements performed in a GPS receiver

in reference to the GPS satellites (and subsequently inferring the position information), where each satellite transmits its individual correlation sequence. The CIR includes both the direct propagation components (line of sight, LOS) and all reflection and scattering components (non line of sight, NLOS) from objects in the environment (Figure 26). The channel model parameters and their values can be derived and determined from the results.

Figure 26: Operating principle of time domain channel sounding
The channel impulse response (CIR) is measured by emitting an electromagnetic "ping" at the frequency of interest and capturing all returning signal components.
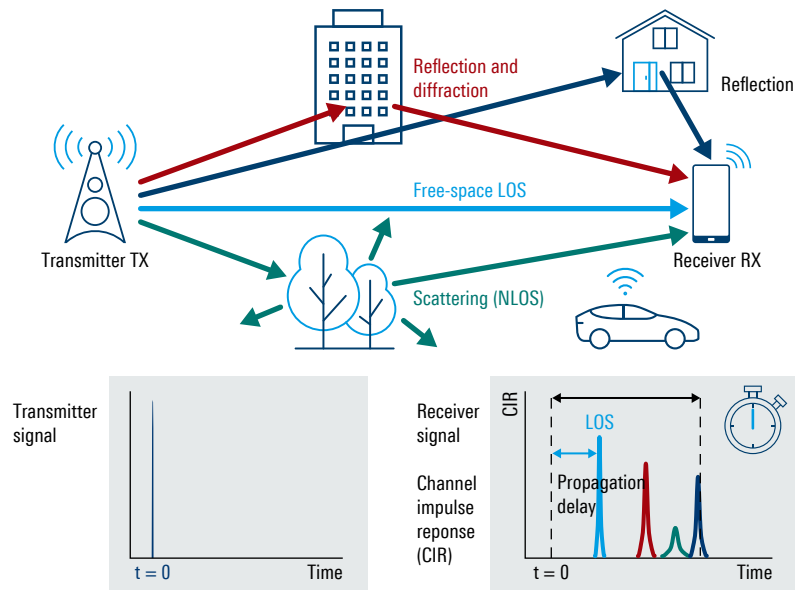
As a rule, objects are only "physically visible" to electromagnetic waves and act as reflectors or scatterers when they are at least as large as the wavelength of the incident wave. This means that at higher frequencies such as 30 GHz, objects with dimensions in the centimeter range already act as reflectors.

Collaborative research
Rohde & Schwarz has many years of experience in channel sounding projects, including a high-resolution channel measurement campaign at 67 GHz in a street canyon in Tokyo, Japan [71]. In 2019, the focal point of a 3GPP research initiative was the development of new 5G channel models in industrial scenarios such as production environments. To support the 3GPP efforts, Rohde & Schwarz in collaboration with the Fraunhofer Heinrich Hertz Institute (HHI) carried out measurements in its Memmingen and Teisnach plants, not only in the 28 GHz and 66 GHz millimeterwave frequency bands but also in the 3.7 GHz to 3.8 GHz band designated for private campus networks in Germany [72].

6.2 Time domain channel sounding at 300 GHz

For 6G, the focus is on channels at significantly higher frequencies. In a collaborative effort with the Fraunhofer HHI and the Fraunhofer Institute for Applied Solid State Physics (IAF), a research setup was developed that enables signal generation and analysis in the range from 275 GHz to 325 GHz with a bandwidth of 2 GHz [73]. The signal can be used to perform channel measurements and also modulated with novel waveforms for transmission experiments. Figure 27 and Figure 28 show the test setup. One of the key technologies from the IAF are InGaAs mHEMT MMICs (see Chapter 5.1) for extremely low-noise and broadband applications at room temperature.

Test setup for propagation delay measurements between transmitter and receiver

The measurements were captured using an instrument based time domain channel sounder as shown in Figure 27. On the transmitter side (TX), an R&S®SMW200A broadband vector signal generator produces a digital baseband "ping sequence" with a bandwidth of 2 GHz (suitable for autocorrelation) at an intermediate frequency (IF). The single-sideband upconverter (incorporating the terahertz transceiver from Fraunhofer IAF) raises this to the wanted RF transmit frequency, with an R&S®SGS100A acting as a local oscillator (LO) source. On the receiver side (RX), the antenna signal is amplified and mixed into the IF domain with a downconverter and LO generator. The IF signal is sampled by the R&S®FSW signal and spectrum analyzer and the I/Q samples are stored for further processing. The transmitter and receiver are synchronized with two rubidium based reference clocks and trigger units (synchronomat) enabling coherent measurements and allowing evaluation of phase and coherent averaging as well as determination of the absolute time of flight. [73] shows further setup details.

Initial measurements at 300 GHz with this test system demonstrated its wide dynamic range, which is unrivaled in this frequency range (Figure 28). The following sections discuss joint measurement campaigns that were carried out with the Fraunhofer HHI in various environmental scenarios for systematically characterizing the subterahertz frequency range.

Figure 27: Block diagram of the 300 GHz channel sounding system
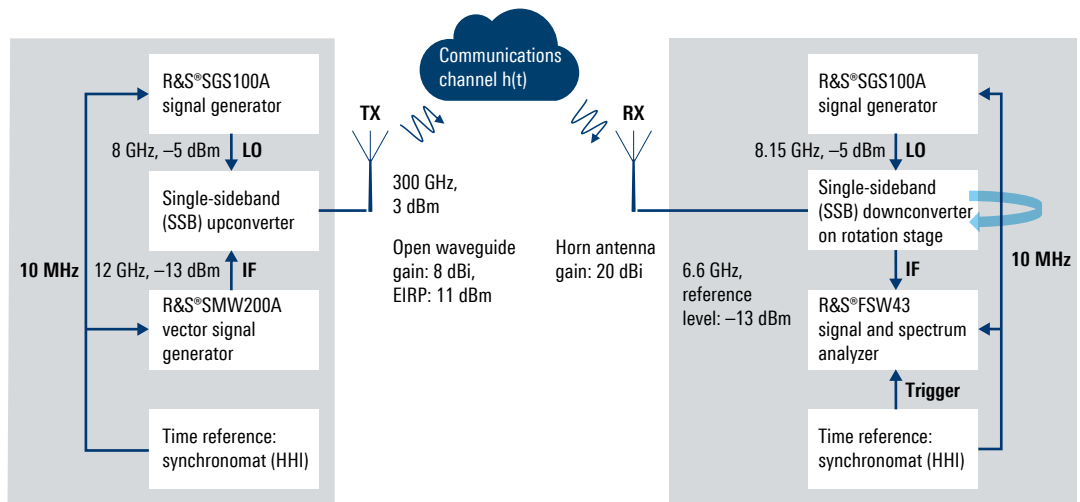
Figure 28: Channel impulse response (CIR) of indoor environment at 300 GHz

Test setup for channel measurements at 300 GHz with the R&S®SMW200A vector signal generator, R&S®SGS100A signal generator and R&S®FSW43 signal and spectrum analyzer. A transceiver with an integrated horn antenna is shown at the top of the picture. The setup can be used in channel sounding for channel characterization as well as for transmission experiments with new waveforms (left). Channel impulse response (CIR) at 300 GHz in an indoor environment with multiple reflections (right). The distance between the transmitter and receiver was approximately 4 m. The pronounced shoulder with many reflections is typical for a very confined (small volume) indoor environment. An electromagnetic wave travels approximately 30 cm in 1 ns.
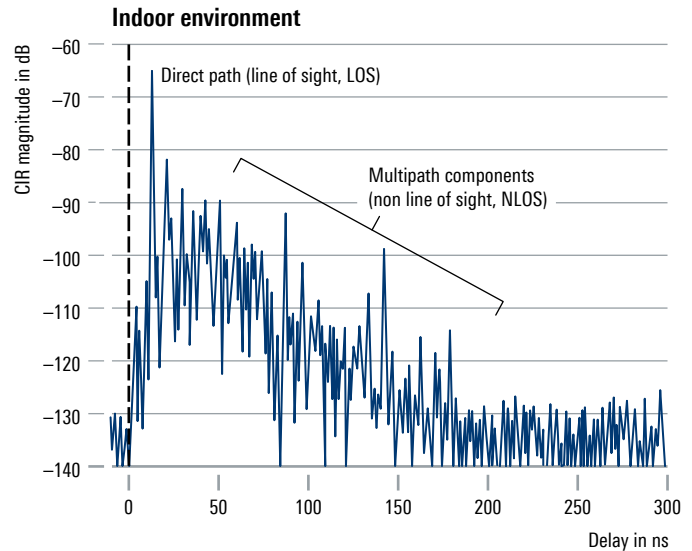
6.3 THz channel measurements at Rohde & Schwarz headquarters in Munich

The characterization of the channel sounding system at 300 GHz [73] described above and the initial measurements using the system were carried out on the premises of the Fraunhofer Heinrich Hertz Institute (HHI). The results were published in [74] for the outdoor scenario and in [75] for the indoor conference room scenario.

Recently, a more systematic study of the channel propagation characteristics at sub-THz frequencies (158 GHz and 300 GHz) was conducted at Rohde & Schwarz headquarters in Munich. The frequencies were chosen in accordance with ongoing future 6G network discussions. The study focused on two representative scenarios: A street canyon like (urban micro-cellular UMi) outdoor scenario in a corridor between two R&D buildings, and an indoor measurement campaign in an atrium similar to a shopping mall or airport scenario.

Figure 29 shows a block diagram of the correlative channel sounder for 158 GHz. This is similar to the setup at 300 GHz (Figure 27). With the applied time domain channel sounder, the measurement duration is short. This allows multiple measurement iterations to be performed covering the complete spatial angle of 360° at numerous positions in the measurement campaign.

Figure 29: Block diagram of the channel sounding measurement setup for 158 GHz
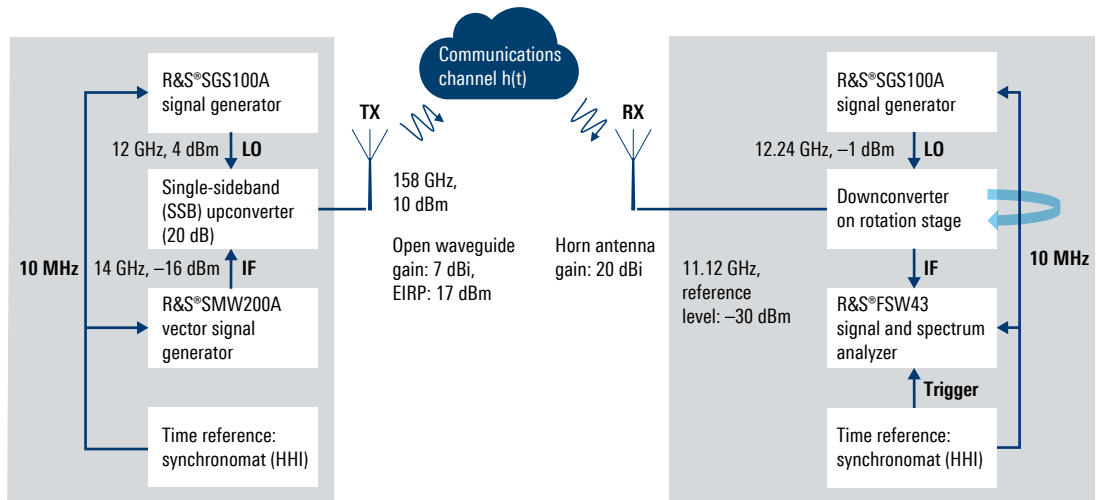
At the **transmitter (TX)**, the setup comprises a single-sideband upconverter and an amplifier connected to an open waveguide with a gain of 7 dBi. The R&S®SMW200A vector signal generator provides a precomputed sounding sequence at an intermediate frequency (IF) of 14 GHz. The used sounding sequence is a Frank-Zadoff-Chu sequence with a length of 100 μs and bandwidth of $B = 2$ GHz (and a corresponding time resolution of $\tau = 1/B = 0.5$ ns).

The **receiver (RX)** consists of an R&S®FSW43 signal and spectrum analyzer and a downconverter that is fed by an LO generator at 12.24 GHz. A horizontally polarized E-plane horn antenna with 20 dBi antenna gain and an opening angle of approx. 15° in the E-plane (azimuth plane) serves as the receive antenna. The D band frontend downconverts the received signal to an IF at 11.12 GHz. The signal analyzer samples the IF signal with a frequency of 2.5 GHz where one measurement covers a total number of 250 periods of the sequences. The receiving antenna and downconverter are mounted on a precision rotation stage to allow angle-resolved measurements with respect to the azimuth angle. The receiver was mounted on a cart (camera dolly) for easy and precise movement to the different receiver positions (Figure 31). Since the used antenna has a beamwidth of approx. 15°, the radio channel is sampled in steps of 15° in the azimuth angle domain at the receiver.

All instruments are connected to a time reference (Fraunhofer HHI synchronomat) to ensure coherent sampling between the transmitter and receiver. Besides a 10 MHz reference signal derived from a high-precision rubidium atomic clock, the synchronomat also enables simultaneous and coherent triggering at the transmitter and receiver.

The received I/Q time domain samples were transferred from the signal analyzer as raw measurement data to a computer after completion of the measurements. Data post-processing includes resampling and filtering, estimation of the common phase drift per sequence period and compensation of the phase drift, coherent averaging of all sequence periods, correlation and application of amplitude and phase corrections by using back-to-back calibration measurement data. The results are generic calibrated channel impulse responses (CIR), sampled at the Nyquist rate and with magnitudes corresponding to the gain of the communications channel (including the antennas) and delays corresponding to the time of flight.

Table 3: Channel sounding measurement parameters at 158 GHz and 300 GHz

Measurement parameters	Value at 158 GHz	Value at 300 GHz
Frequency	158 GHz	300 GHz
Bandwidth	2 GHz	2 GHz
Temporal resolution	0.5 ns	0.5 ns
Autocorrelation sequence	Frank-Zadoff-Chu	Frank-Zadoff-Chu
Period length	200 000 samples	200 000 samples
Period duration (maximum measurable channel length)	100 µs	100 µs
Number of measured periods	250	250
Measurement duration	25 ms	25 ms
Theoretical processing gain	77 dB	77 dB
Dynamic range	> 70 dB	> 70 dB
Transmit power	10 dBm	3 dBm
TX antenna gain	8 dBi	8 dBi
Effective isotropic radiated power (EIRP)	18 dBm	11 dBm
RX antenna gain	20 dBi	20 dBi
Angular resolution	15° (24 steps)	15° (24 steps)

Table 3 summarizes the essential technical parameters for the time domain channel sounder. Using a configuration with perfect complex correlation sequences (Frank-Zadoff-Chu sequences) and with additional coherent averaging after estimation and compensation of drift due to phase noise enables a large processing gain and an exceptionally wide dynamic range. Fundamental assessments of the utilized time domain channel sounding principle can be found in [76].

The following section describes some of the preliminary results. A more detailed quantitative analysis is in preparation.

6.4   Measurement scenarios and results

The measurements were conducted at Rohde&Schwarz headquarters in Munich, Germany. They represented an urban micro street canyon scenario and an indoor shopping mall/airport scenario (Figure 30). The outdoor measurements were performed between the two gray shaded buildings on the left. The width of the street is 15.5 m and the height of the surrounding buildings is approx. 20 m.

Figure 30: Map of the investigated scenarios

Street canyon (left), indoor shopping mall/airport scenario (right). The positions of the fixed transmitter (TX) are marked with red stars and the different positions of the receiver (RX) with green stars.
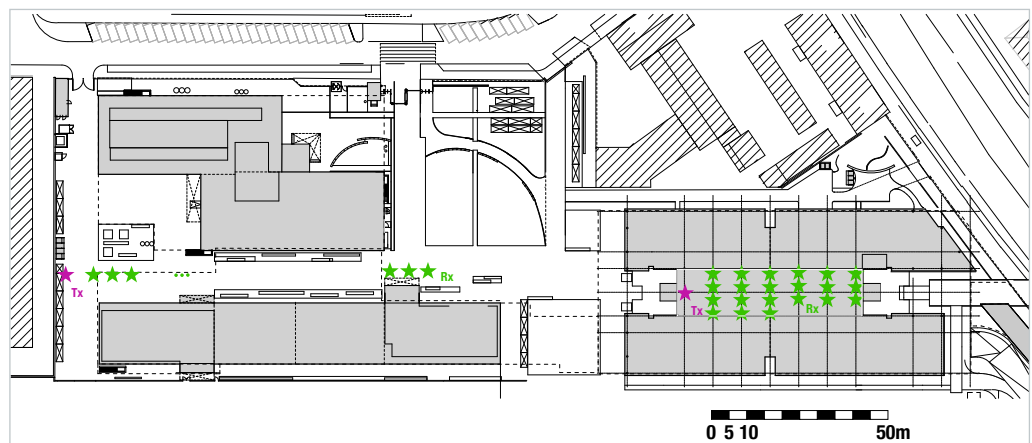
6.4.1 Outdoor street canyon scenario (urban micro-cellular UMi)

The first measurement scenario was located in a corridor between two R&D buildings resembling a street canyon scenario (urban micro-cellular UMi) as shown in Figure 30 and Figure 31. The stationary transmitter (TX) was placed at a height of 1.5 m at a bicycle stand (red star on left side of Figure 30) at the end of the corridor. There, the scenery leads into a more open space with a small plaza and isolated trees (Figure 31). The receiver (RX) including the T&M equipment was mounted on a wireless platform (camera dolly) at a height of 1.5 m and positioned at measurement positions at various distances from the transmitter up to a maximum distance of 170 m (Figure 32). Most of the measurements were in a line of sight (LOS) situation.

The example measurements in Figure 31 show the CIR for aligned antennas at a distance of 30 m for 158 GHz and 300 GHz. The first peak with a delay (time of flight) of 0.1 μs represents the LOS path, corresponding to a distance of 30 m. Multipath components are also visible and more pronounced at 158 GHz than at 300 GHz.

Figure 31: Angle-resolved CIR THz channel measurements at 158 GHz and 300 GHz (D band) in an outdoor street canyon environment at Rohde & Schwarz headquarters in Munich

The left photo shows the transmitter (TX) perspective at the end of the street canyon (see also Figure 30). The right photo shows the RX setup mounted on a wireless platform (camera dolly) for measurements at variable positions. Measurement examples are shown below with channel impulse responses at 30 m distance from the transmitter at 158 GHz (left) and at 300 GHz at the same position (right). Note that 1 μs delay corresponds to 300 m distance.
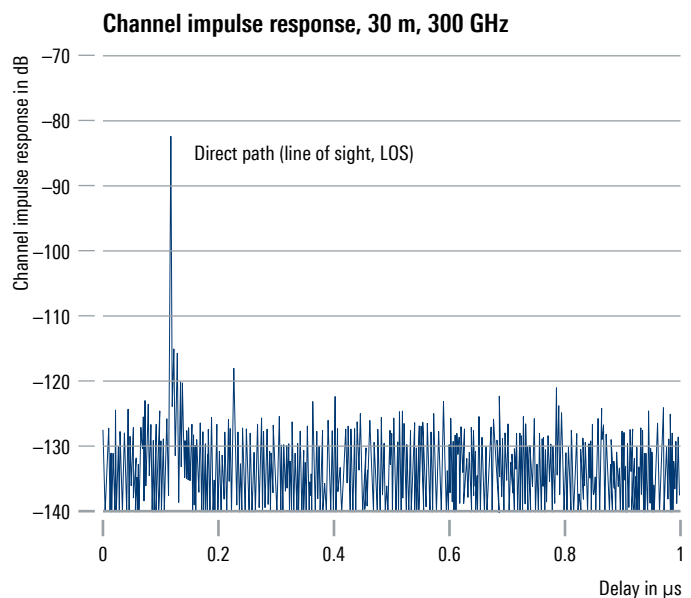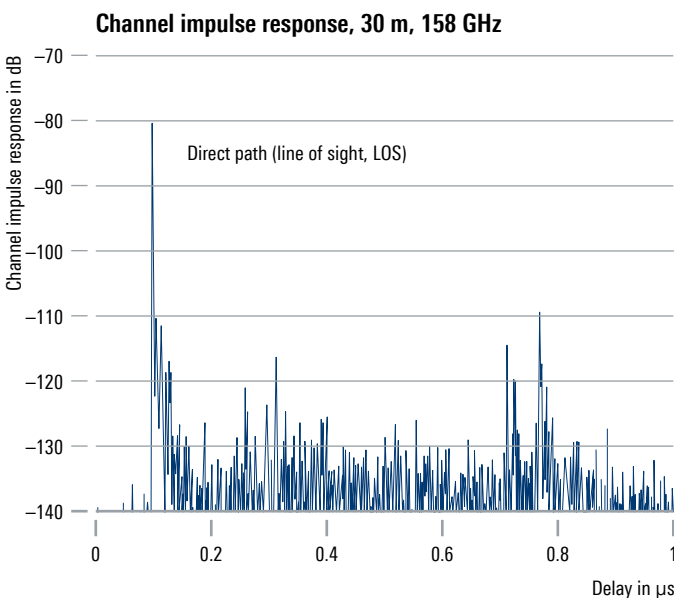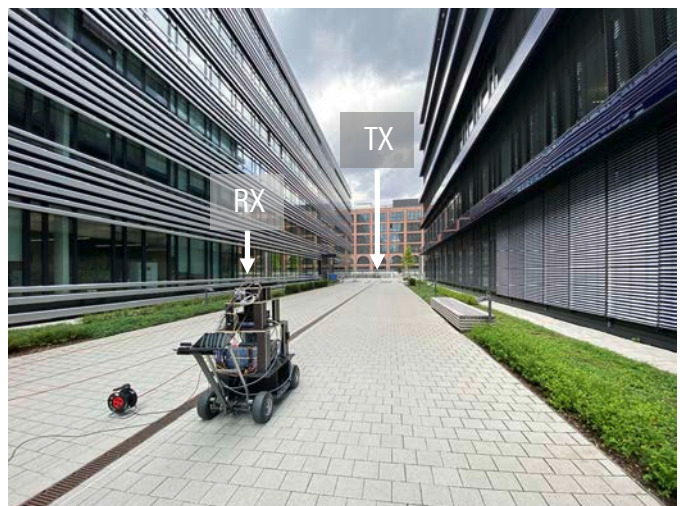
Figure 32 shows the instantaneous CIRs in an outdoor scenario at 158 GHz at various distances from 10 m to 170 m combined into one plot. These measurements cover the complete street length between the two buildings. The antennas were always aligned. From this set of large-scale measurements, the path loss exponent can be derived. The multipath components at larger delays are present almost over the complete measurement setup.

Figure 32: Large-scale outdoor street canyon scenario measurements
The graph shows the CIRs at 158 GHz with aligned antennas over the distance from 10 m to 170 m.

Channel impulse responses, 158 GHz
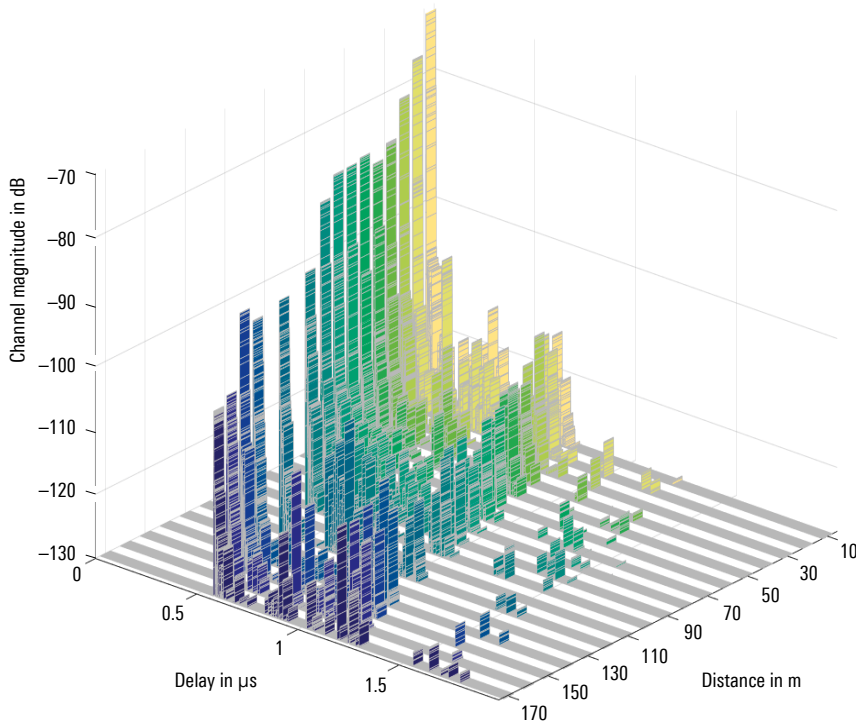
Angle-resolved measurements

Further evaluation of the measured data sets involved analysis of the angular information. At each measurement point, the receiver was rotated to 24 equally spaced angular positions, resulting in spatial scanning of the radio channel in the azimuth plane with 15° resolution.

Figure 33 shows the result of a path estimation for both frequencies (158 GHz and 300 GHz) at the same measurement point (30 m, outdoor). The angle axis represents a cyclic dimension, meaning the first and last rows in these plots are identical. This is also reflected by the colors. For these evaluations, proper control of the noise threshold is necessary in order to clearly discriminate the signal paths from noise. For the example given in Figure 33, the absolute noise thresholds were set to –120 dB for 158 GHz and to –118 dB for 300 GHz.

Estimated paths, 30 m, 158 GHz
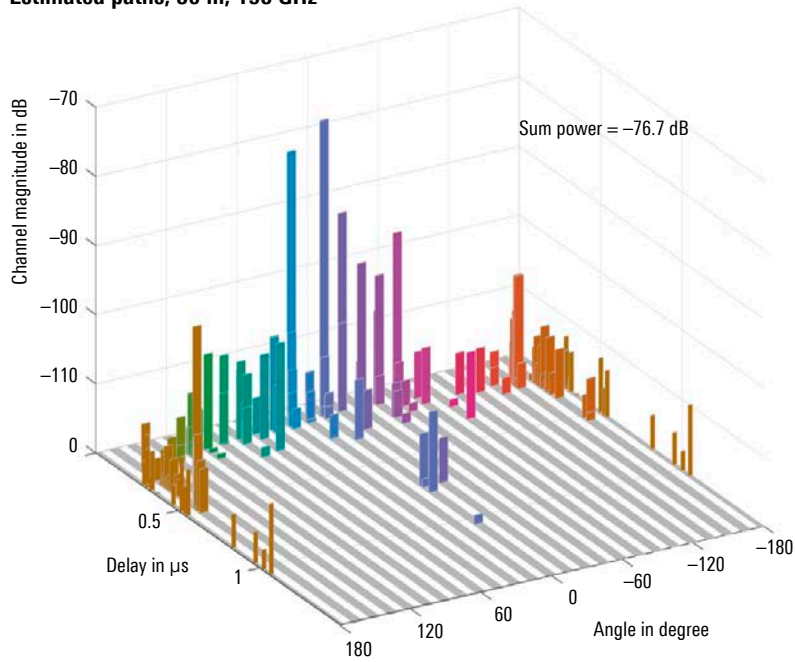
Estimated paths, 30 m, 300 GHz
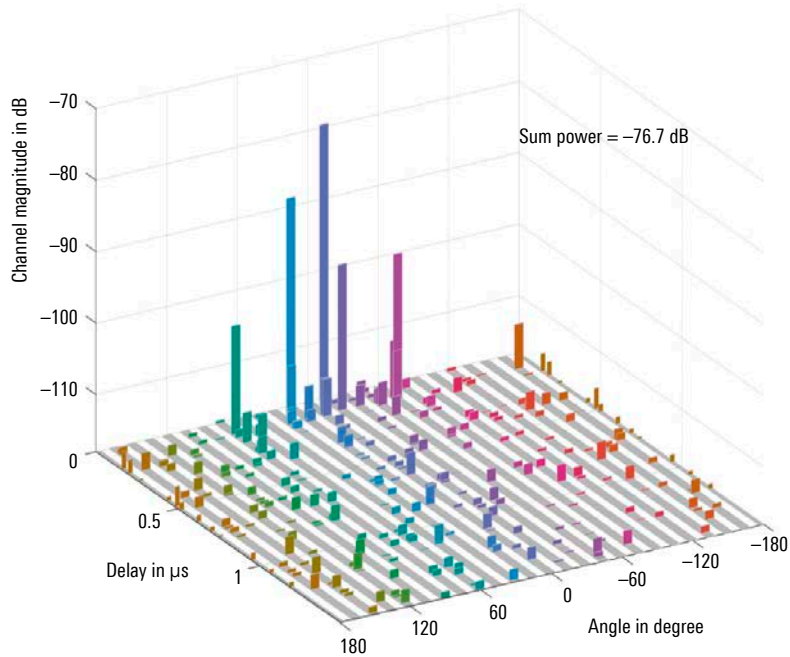
Based on this path estimation, it is possible to sum up the overall received power (i.e. effective overall path gain) from all paths. This is also indicated in the plots. Although the channel at 300 GHz is much sparser than the channel at 158 GHz, we can clearly see that there is not a large difference in overall power. We would expect the overall power at 300 GHz to be around 6 dB less, compared to 158 GHz. However, this is not the case. We can thus conclude that the additional paths at 158 GHz could be resolved owing to the high sensitivity of the measurement principle, but they do not significantly contribute

to the overall power. Statistical parameters such as the root mean square (RMS) delay spread and the RMS angular spread can also be evaluated from these results.

Further results for the channel measurement campaign performed in an urban micro-cellular (UMi) street canyon scenario at 158 GHz and 300 GHz as described above are also summarized in [77].

6.4.2 Indoor shopping mall/airport scenario in R&D building atrium

The indoor measurements were performed in a large open space in the building shown on the right side of Figure 30 and in the photo of Figure 34. The scenario resembles a shopping mall/airport scenario. The size of the hall is approx. 52 m x 13 m with a ceiling height of around 20 m. The transmit antenna (TX) was configured at a fixed position in front of the elevators at the building entrance at a height of 1.5 m. The receiver was mounted on a wireless platform (antenna height 1.5 m) and moved to distinct positions on a rectangular grid covering the complete floor area.

Figure 34: Photograph of the indoor atrium scenario (shopping mall/airport) with the receiver on a rotation stage in the front facing towards the transmitter position at the elevators in the back (see also Figure 30)
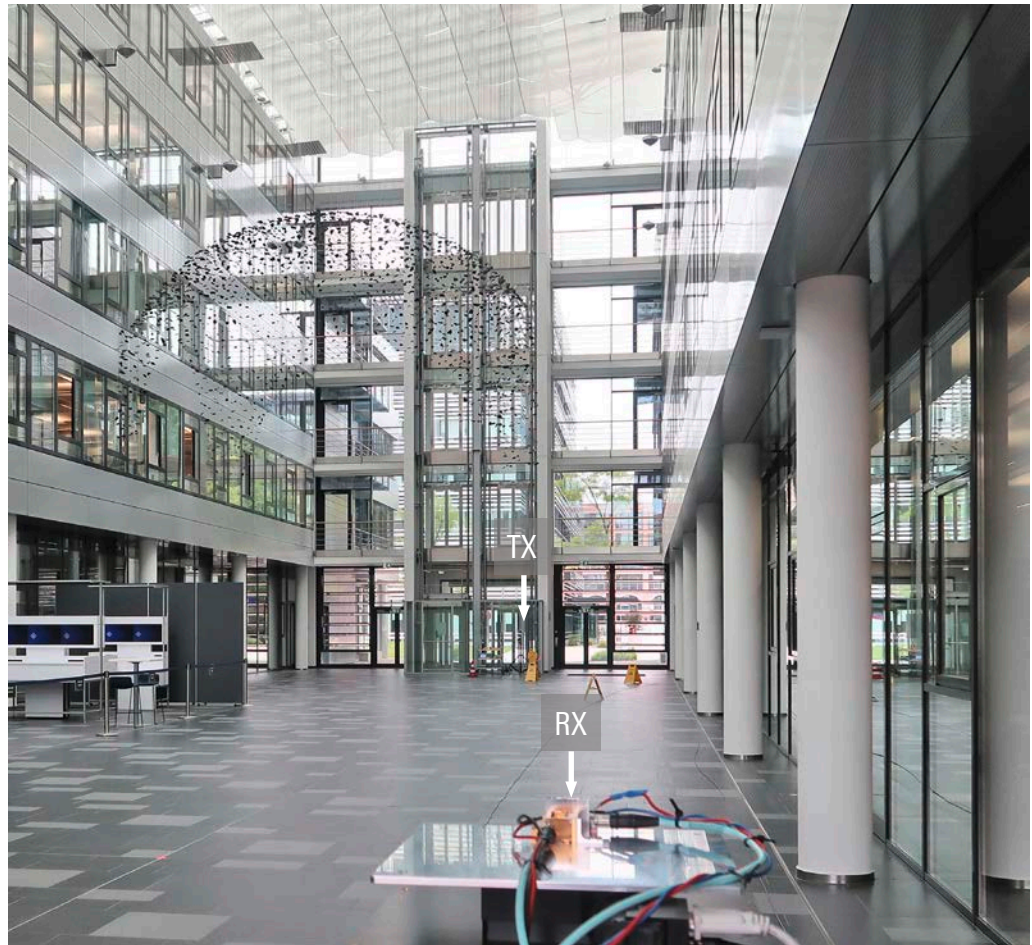
Figure 35 shows the angle-resolved estimated paths at one particular position (in the rect-angular grid) with the LOS peak and a number of multipath components. It is an example of indoor measurements at 158 GHz and a distance of 40 m. As expected, there are more multipath components from different directions contributing to higher overall received power compared to outdoor measurements (–71.4 dB at 40 m versus –75.1 dB at 30 m).

Another interesting result representation can be visualized by means of a rose plot as shown in Figure 35 (right). Here, each "pie" represents the overall power in the respective angle bin, normalized to the overall power. Single contributions from distinct paths within one angle bin are depicted by dots. Again, we can clearly see that only one or two angle bins account for almost all of the overall power and that within one bin, only a few paths contribute significantly.

Although most of the power is received from the line of sight (LOS) direction, significant multipaths arrive from all measured azimuth directions. A more detailed statistical analy-sis of the collected measurement data in terms of directional channel gain can be found in [78].

Figure 35: Estimated paths of one particular indoor position at 158 GHz for the atrium scenario (shopping mall/airport) with an angular range covering −180° to 180°

In the rose plot on the bottom, the same data set is shown in a polar plot where each dot corresponds to one peak and the triangle ("pie") represents the overall power in the respective angle bin. A number of multipath components can be observed.

Estimated paths, position 4, 158 GHz
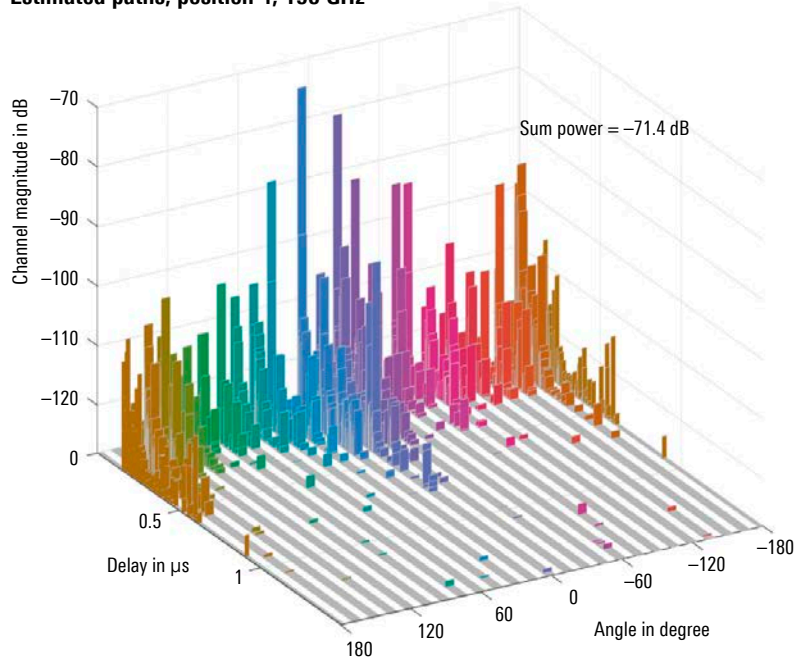
Estimated paths, position 4, 158 GHz
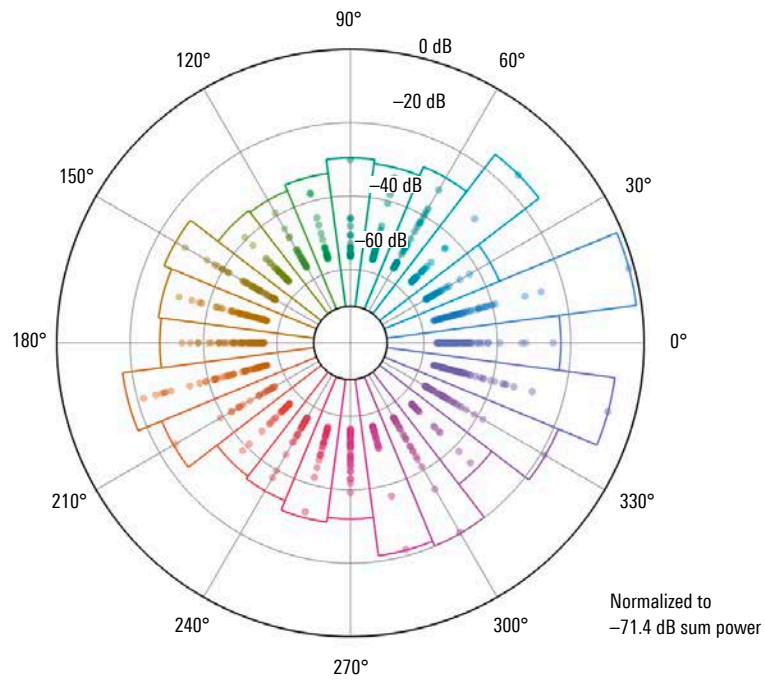
7 CONCLUSION

THz technology and applications represent just one potential building block for future 6G wireless communications. Nevertheless, the technology promises to be indispensable – not only to achieve target requirements in terms of maximum throughput on the Tbit/s level as well as extremely low latencies, but also to realize intriguing novel applications. Envisioned 6G use cases span a plethora of applications ranging from communications, spectroscopy, imaging and sensing. However, successful commercial implementation will require viable business models that have yet to be developed.

THz technology may need some time to reach large-scale commercialization after the targeted 6G network rollout around 2030. Nevertheless, the initiated research activities have already spurred innovation in terms of the rapid evolution of high frequency semiconductor technologies for RF electronics as well as promising new devices.

While semiconductor technology continues to evolve towards extremely high frequencies, the technical challenges are known and inherited from mmWaves. Namely, they involve efficiency and power consumption. In comparison to mmWaves, the challenges only intensify in the terahertz spectral region due to the even shorter range of radio wave propagation. However, such problems can be mitigated by focusing signals through beamforming, which involves accommodating an even larger number of antennas in a small volume to produce pinpoint beams. Although outdoor and indoor terahertz use cases are feasible, indoor use cases are likely to dominate.

Using photonic technologies to generate THz waves could represent an alternative technology evolution branch with the potential to transfer the existing power efficiency of optoelectronic devices into the THz frequency region. Furthermore, by miniaturizing today's lab setups into photonic integrated circuits (PIC), these approaches could become mainstream. It will be fascinating to see which technology will eventually prevail or which of the approaches will be used for which dedicated application.

The next milestone for initial 6G technology trials and feasibility studies is the World Radio Conference (WRC) in 2023. While decisions about the 6G spectrum will not be made in 2023, WRC23 will set the agenda for the next WRC in 2027 – when 6G standardization will be in full swing. That is why research activities in industry and academia are striving to have proof in hand by 2023 that terahertz communications is both usable and technically feasible. This includes THz channel measurement campaigns as described in the last chapter to understand the propagation characteristics and develop channel models for this novel communications frequency region – as well as the terahertz radio links that have already been demonstrated by various companies and research institutions.

Rohde & Schwarz has been a close partner and leading test and measurement supplier for industry and academia since the beginning of the digital wireless communications era. Today, the company is already providing solutions and expertise to accompany 6G research projects, including THz research, and pave the way towards commercialization of the next wireless communications standard.

8 REFERENCES

[1] "5G Evolution and 6G," NTT DOCOMO, Inc., White Paper, January 2022 (Version 4.0).

[2] "Key drivers and research challenges for 6G ubiquitous wireless intelligence," 6G flagship research program, University of Oulu, Finland, 2019.

[3] Samsung, "6G The Next Hyper-Connected Experience for All," White Paper, 2021.

[4] The 5G Infrastructure Association, "European Vision for the 6G Network Ecosystem," White Paper, 2021.

[5] Nokia Bell Labs, "Communications in the 6G Era," White Paper, 2021.

[6] 6G Flagship, University of Oulu, "White Paper on RF Enabling 6G - Opportunities and Challenges from Technology to Spectrum," 6G Research Visions, No. 13, April 2021.

[7] MediaTek Inc., "6G Vision Whitepaper," January 2022.

[8] IMT-2030 (6G) Promotion Group, "6G Vision and Candidate Technologies," CAICT, MIIT, China, June 2021.

[9] National Institute of Information and Communications Technology (NICT), "Beyond 5G/6G White Paper," Tokyo, August 2021.

[10] KDDI Research, Inc., "Beyond 5G/6G White Paper ver.2.0.1," October 2021.

[11] Innovative Optical Wireless Network Global Forum (IOWN GF), "IOWN GF System and Technology Outlook," 2021.

[12] 5G Americas, "Mobile Communications towards 2030 (White Paper)," November 2021.

[13] H. Chun, A. Gomez, C. Quintana et al., "A Wide-Area Coverage 35 Gb/s Visible Light Communications Link for Indoor Wireless Applications," Nature Scientific Reports, vol. 9, p. 4952, 2019.

[14] Juan Yin et al., "Satellite-based entanglement distribution over 1200 kilometers," Science, vol. 356, no. 6343, pp. 1140 to 1144, 2017.

[15] National Institute of Information and Communications Technology (NICT), "Quantum Network White Paper," Tokyo, August 2021.

[16] ETSI, "Industry Specification Group (ISG) on Reconfigurable Intelligent Surfaces (RIS)," October 2021. [Online]. Available: https://www.etsi.org/committee/ris.

[17] V. Joshi, M. Le Gallo, S. Haefeli et al., "Accurate deep neural network inference using computational phase-change memory," Nature Communications, vol. 11, p. 2473, 2020.

[18] A. Sebastian, M. Le Gallo et al., "Memory devices and applications for in-memory computing," Nature Nanotechnology, vol. 15, pp. 529 to 544, 2020.

[19] F.-L. Luo, Machine Learning for Future Wireless Communications, Wiley-IEEE Press, 2020.

[20] ETSI White Paper #34, "Artificial Intelligence and future directions for ETSI," ETSI, June 2020.

[21] C. E. Shannon, "A Mathematical Theory of Communication," The Bell System Technical Journal, vol. 27, pp. 379 to 423, 623 to 656, 1948.

[22]   ITU Radiocommunication (ITU-R), "Radio Regulations, Articles, Edition of 2020," ITU, 2020.

[23]   ITU, "World Radiocommunication Conference 2019 (WRC19) Final Acts," Oct-Nov 2019.

[24]   "IEEE 802.15 WPAN™ Terahertz Interest Group (IGthz),"
        [Online]. Available: https://grouper.ieee.org/groups/802/15/pub/SCTHz.html.

[25]   M. Naftaly, N. Vieweg and A. Deninger, "Industrial Applications of Terahertz Sensing: State of Play,"
        Sensors, vol. 19, p. 4203, 2019.

[26]   VDI / VDE, "Terahertzsysteme und Anwendungsfelder, VDI-Statusreport," VDI / VDE-Gesellschaft Mess- und
        Automatisierungstechnik, March 2020.

[27]   R. W. Wilson, K. B. Jefferts and A. A. Penzias, "Carbon Monoxide in the Orion Nebula," Astrophysical Journal,
        vol. 161, pp. L43 to L44, July 1970.

[28]   B. Thomas et al., "The Ice Cloud Imager Front End Receivers onboard MetOp-SG satellite – Preliminary Design
        and Results," in 28th International Symposium on Space Terahertz Technology (ISSTT 2017),
        Cologne, Germany, 2017.

[29]   J. A. Francis, "Vapor Storms," Scientific American, vol. 325, no. 5, pp. 26 to 33, November 2021.

[30]   B. Thomas et al., "Digitally tunable 150 GHz Local Oscillator chain for the Submillimeter Wave Instrument
        onboard the ESA JUICE mission," in Proceedings of the 30th International Symposium on Space Terahertz
        Technology (ISSTT2019), Gothenburg, Sweden, 2019.

[31]   Ericsson, "Microwave backhaul beyond 100 GHz," Ericsson Technology Review, February 2017.

[32]   A. S. Hamza, J. S. Deogun and D. R. Alexander, "Wireless Communication in Data Centers: A Survey,"
        IEEE Communications Surveys & Tutorials, vol. 18, no. 3, pp. 1572 to 1595, 2016.

[33]   The Event Horizon Telescope Collaboration et al., "First M87 Event Horizon Telescope Results. IV. Imaging the
        Central Supermassive Black Hole," The Astrophysical Journal Letters, vol. 875, no. 1, 2019.

[34]   M. Tonouchi, "Cutting-edge terahertz technology," Nature Photonics, vol. 1, p. 97 to 105, February 2007.

[35]   A. Rumiantsev, T. Naing Swe and A. Henkel, "Achieving Metrology-Level Accuracy When Making THz
        Measurements," in The Latest in mmWave and THz Test and Measurement Technology,
        https://www.microwavejournal.com/articles/27082, Microwave Journal, December 2021.

[36]   Th. de Graauw et al., "The Herschel-Heterodyne Instrument for the Far-Infrared (HIFI),"
        Astronomy and Astrophysics, vol. 518, p. id. L6, July 2010.

[37]   R. Stuhlfauth and H. Mellein, "Over-the-air RF conformance measurements on 5G NR devices,"
        Rohde & Schwarz white paper, 2021.

[38]   B. Derat, S. Schmitz, S. Lachner, M. A. Campo and S. Bruni, "Numerical Modeling and Experimental Validation of
        a D-band Lens-Based Antenna Design for Beyond 5G Communications," 2020 Antenna Measurement Techniques
        Association Symposium (AMTA), pp. 1 to 5, 2020.

[39]   J. Faist, F. Capasso, D. L. Sivco, C. Sirtori, A. L. Hutchinson and A. Y. Cho, "Quantum Cascade Laser," Science,
        vol. 264, no. 5158, pp. 553 to 556, 1994.

[40]   R. Köhler, A. Tredicucci and F. Beltram et al., "Terahertz semiconductor-heterostructure laser," Nature,
        vol. 417, pp. 156 to 159, 2002.

[41] K. Fujita et al., "Sub-terahertz and terahertz generation in long-wavelength quantum cascade lasers," Nanophotonics, vol. 8, no. 12, pp. 2235 to 2241, 2019.

[42] A. Khalatpour, A. K. Paulsen, C. Deimert et al., "High-power portable terahertz laser systems," Nature Photonics, vol. 15, pp. 16 to 20, 2021.

[43] T. Nagatsuma, G. Ducournau and C. Renaud, "Advances in terahertz communications accelerated by photonics," Nature Photonics, vol. 10, pp. 371 to 379, 2016.

[44] L. Liebermeister, S. Nellen, B. Globisch et al., "Optoelectronic frequency-modulated continuous-wave terahertz spectroscopy with 4 THz bandwidth," Nature Communications, vol. 12, p. 1071, 2021.

[45] S. Nellen, T. Ishibashi, A. Deninger et al., "Experimental Comparison of UTC- and PIN-Photodiodes for Continuous-Wave Terahertz Generation," Journal of Infrared, Millimeter, and Terahertz Waves, vol. 41, pp. 343 to 354, 2020.

[46] T. Ishibashi, Y. Muramoto, T. Yoshimatsu and H. Ito, "Unitraveling-Carrier Photodiodes for Terahertz Applications," IEEE Journal of Selected Topics in Quantum Electronics, vol. 20, no. 6, pp. 79 to 88, 2014.

[47] T. Ishibashi and H. Ito, "Uni-Traveling Carrier Photodiodes: Development and Prospects," IEEE Journal of Selected Topics in Quantum Electronics, vol. 28, no. 2, pp. 1 to 6, March-April 2022.

[48] H. Song, K. Ajito, Y. Muramoto, A. Wakatsuki, T. Nagatsuma and N. Kukutsu, "Uni-Travelling-Carrier Photodiode Module Generating 300 GHz Power Greater Than 1 mW," IEEE Microwave and Wireless Components Letters, vol. 22, no. 7, pp. 363 to 365, July 2012.

[49] P. Latzel et al., "Generation of mW Level in the 300-GHz Band Using Resonant-Cavity-Enhanced Unitraveling Carrier Photodiodes," IEEE Transactions on Terahertz Science and Technology, vol. 7, no. 6, pp. 800 to 807, Nov. 2017.

[50] J. Webber et al., "Terahertz Band Communications With Topological Valley Photonic Crystal Waveguide," Journal of Lightwave Technology, vol. 39, no. 24, pp. 7609 to 7620, December 2021.

[51] R. Gotti, T. A. Puppe, Y. Mayzlin et al., "Comb-locked frequency-swept synthesizer for high precision broadband spectroscopy," Nature Scientific Reports, vol. 10, p. 2523, 2020.

[52] T. Fortier and E. Baumann, "20 years of developments in optical frequency comb technology and applications," Communication Physics, vol. 2, no. 153, 2019.

[53] A. D. J. Fernandez Olvera, B. L. Krause and S. Preu, "A True Optoelectronic Spectrum Analyzer for Millimeter Waves With Hz Resolution," IEEE Access, vol. 9, pp. 114339 to 114347, 2021.

[54] A. D. J. Fernandez Olvera, A. K. Mukherjee and S. Preu, "A Fully Optoelectronic Continuous-Wave 2-Port Vector Network Analyzer Operating From 0.1 THz to 1 THz," IEEE Journal of Microwaves, vol. 1, no. 4, pp. 1015 to 1022, Oct. 2021.

[55] V. K. Chinni et al., "Single-channel 100 Gbit/s transmission using III–V UTC-PDs for future IEEE 802.15.3d wireless links in the 300 GHz band," Electronics Letters, vol. 54, pp. 638 to 640, 2018.

[56] T. Nagatsuma et al., "Real-time 100-Gbit/s QPSK transmission using photonics-based 300-GHz-band wireless link," 2016 IEEE International Topical Meeting on Microwave Photonics (MWP), pp. 27 to 30, 2016.

[57] C. Castro et al., "32 GBd 16QAM Wireless Transmission in the 300 GHz Band using a PIN Diode for THz Upconversion," Optical Fiber Communications Conference and Exhibition (OFC), pp. 1 to 3, 2019.

[58] I. Dan, G. Ducournau, I. Kalfass et al., "A 300-GHz Wireless Link Employing a Photonic Transmitter and an Active Electronic Receiver With a Transmission Bandwidth of 54 GHz," IEEE Transactions on Terahertz Science and Technology, vol. 10, no. 3, pp. 271 to 281, May 2020.

[59] S. Koenig, D. Lopez-Diaz, J. Antes et al., "Wireless sub-THz communication system with high data rate," Nature Photonics, vol. 7, pp. 977 to 981, 2013.

[60] D. Stanze, A. Deninger, A. Roggenbuck, et al., "Compact CW Terahertz Spectrometer Pumped at 1.5 μm Wavelength," Journal of Infrared, Millimeter, and Terahertz Waves, vol. 32, pp. 225 to 232, 2011.

[61] N. Vieweg, F. Rettich, A. Deninger et al., "Terahertz-time domain spectrometer with 90 dB peak dynamic range," Journal of Infrared, Millimeter, and Terahertz Waves, vol. 35, pp. 823 to 832, 2014.

[62] F. Roccaforte and M. Leszczynski, Nitride Semiconductor Technology: Power Electronics and Optoelectronic Devices, Wiley-VCH Verlag GmbH & Co. KGaA, 2020.

[63] S. Nakamura, "Nobel Lecture: Background story of the invention of efficient blue InGaN light emitting diodes," Rev. Mod. Phys., vol. 87, p. 1139, 2015.

[64] M. Cwiklinski, "Design of Millimeter-Wave Power Amplifiers in GaN HEMT Technology," Ph.D. Dissertation, 2021.

[65] H. Wang et al., "Power Amplifiers Performance Survey 2000-Present," https://gems.ece.gatech.edu/PA_survey.html.

[66] B. Gashi et al., "Broadband 400-GHz InGaAs mHEMT Transmitter and Receiver S-MMICs," IEEE Transactions on Terahertz Science and Technology, vol. 11, no. 6, pp. 660 to 675, Nov. 2021.

[67] X. Mei et al., "First Demonstration of Amplification at 1 THz Using 25-nm InP High Electron Mobility Transistor Process," IEEE Electron Device Letters, vol. 36, no. 4, pp. 327 to 329, April 2015.

[68] ITU-R, "Draft working document towards a preliminary draft new Report ITU-R M.[IMT.ABOVE 100 GHz TECHNICAL FEASIBILITY OF IMT IN BANDS ABOVE 100 GHz]," ITU, 2022.

[69] "3GPP TR 38.901 (V16.0.0): Study on channel model for frequencies from 0.5 to 100 GHz," 3rd Generation Partnership Project (3GPP), October 2019.

[70] S. Salous, Radio Propagation Measurement and Channel Modelling, Wiley, 2013.

[71] M. Peter, W. Keusgen, T. Eichler, K. Yanagisawa, K. Kitao, T. Imai, M. Inomata, Y. Okumura and T. Nakamura, "High-Resolution Directional Channel Measurements at 67 GHz and Advanced Analysis of Interactions Using Geometric Information," 2018 IEEE International Symposium on Antennas and Propagation & USNC/URSI National Radio Science Meeting, pp. 77 to 78, 2018.

[72] M. Schmieder, T. Eichler, S. Wittig, M. Peter and W. Keusgen, "Measurement and Characterization of an Indoor Industrial Environment at 3.7 and 28 GHz," 2020 14th European Conference on Antennas and Propagation (EuCAP), pp. 1 to 5, 2020.

[73] M. Schmieder, W. Keusgen, M. Peter, S. Wittig, T. Merkle, S. Wagner, M. Kuri and T. Eichler, "THz Channel Sounding: Design and Validation of a High Performance Channel Sounder at 300 GHz," 2020 IEEE Wireless Communications and Networking Conference Workshops (WCNCW), pp. 1 to 6, 2020.

[74] F. Undi, A. Schultze, W. Keusgen, M. Peter and T. Eichler, "Angle-Resolved THz Channel Measurements at 300 GHz in an Outdoor Environment," 2021 IEEE International Conference on Communications Workshops (ICC Workshops), pp. 1 to 7, 2021.

[75] A. Schultze, F. Undi, M. Peter, W. Keusgen and T. Eichler, "Angle-Resolved THz Channel Measurements at 300 GHz in a Conference Room Environment," 2021 XXXIVth General Assembly and Scientific Symposium of the International Union of Radio Science (URSI GASS), pp. 1 to 4, 2021.

[76] S. Wittig, W. Keusgen, M. Peter and T. Eichler, "On the Dynamic Range of Digital Correlative Time Domain Radio Channel Measurements," arXiv:2008.07805, 2020.

[77] W. Keusgen, A. Schultze, M. Peter and T. Eichler, "Sub-THz Channel Measurements at 158 GHz and 300 GHz in a Street Canyon Environment," in submitted to 2022 Joint European Conference on Networks and Communications & 6G Summit (EuCNC/6G Summit), https://arxiv.org/abs/2203.04404, Grenoble, 2022.

[78] A. Schultze, W. Keusgen, M. Peter and T. Eichler, "Observations on the Angular Statistics of the Indoor Sub-THz Radio Channel at 158 GHz," 2022 IEEE USNC-URSI Radio Science Meeting (Joint with AP-S Symposium), pp. 9 to 10, doi: 10.23919/USNC-URSI52669.2022.9887443, https://ieeexplore.ieee.org/document/9887443, 2022.

Note: All links have been checked and were functional when this document was created. However, we cannot rule out subsequent changes to the links in the reference list.

Rohde & Schwarz

The Rohde & Schwarz technology group is among the trailblazers when it comes to paving the way for a safer and connected world with its leading solutions in test & measurement, technology systems and networks & cybersecurity. Founded more than 85 years ago, the group is a reliable partner for industry and government customers around the globe. The independent company is headquartered in Munich, Germany and has an extensive sales and service network with locations in more than 70 countries.

www.rohde-schwarz.com

Rohde & Schwarz customer support

www.rohde-schwarz.com/support